FlatChem 45 (2024) 100662

Contents lists available at ScienceDirect

FlatChem

journal homepage: www.sciencedirect.com/journal/flatchem

Modification of graphene-based nanomaterials with gamma irradiation as an eco-friendly approach for diverse applications: A review

Nkosingiphile E. Zikalala [a,b], Shohreh Azizi [a,*], Force T. Thema [a,b,f,*], Karen J. Cloete [a,b], Ali.A. Zinatizadeh [d], Touhami Mokrani [e], Nomvano Mketo [c], Malik M. Maaza [a,b]

[a] UNESCO-UNISA Africa Chair in Nanosciences & Nanotechnology Laboratory, College of Graduate Studies, University of South Africa, Muckleneuk Ridge, P.O. Box 392, Pretoria 0002, South Africa
[b] Nanosciences African Network (NANOAFNET)-Materials Research Department, iThemba LABS-National Research Foundation, Somerset West, P.O. Box 722, Cape Town 7129, South Africa
[c] Department of Chemistry, College of Science and Engineering and Technology, Florida Science Campus, University of South Africa, Johannesburg, South Africa
[d] Environmental Research Canter, Department of Applied Chemistry, Razi University, Kermanshah P.O. Box 67144-14971, Iran
[e] Department of Chemical Engineering, University of South Africa, Private Bag X6, Florida, Johannesburg 1709, South Africa
[f] Botswana University of Agriculture and Natural Resources (BUAN), Private Bag 00027 Gaborone, Botswana

ARTICLE INFO

Keywords:
Graphene
γ-irradiation
Modification
Photocatalysis
Energy storage

ABSTRACT

Graphene-based nanomaterials (GBNMs) are versatile due to their large surface area, great mechanical, chemical strength, and excellent electrical properties. The versatility of graphene has increased its applicability therefore several synthesis methods to produce high quality graphene simpler, faster, and cost-effectively are actively explored. The conventional synthesis methods however employ toxic chemicals, high temperatures, and lengthy synthesis times. On the other hand, the gamma (γ) irradiation approach is facile, occurs under ambient conditions and produces graphene composites of high purity. Noteworthy, this technique enables the user to control the synthesis time and total dose, hence minimising the aggregation of the nanomaterial, the main drawback hindering the commercial production of GBNMs. γ-radiolysis synthesized GBNMs exhibit superior optical and electrical properties and hence improved supercapacitance, catalytic, and sensing abilities. Although other reviews addressed the γ-ray synthesis of metallic nanomaterials, polymers, as well as usage of a variety of radiation techniques to fabricate graphene composites, this review focuses solely on the synthesis and modifications of GBNMs via the γ-synthesis technique. Properties of graphene and conventional methods used to reduce graphene oxide (GO) to graphene as well as their shortcomings are highlighted. This is followed by detailing the γ-radiation synthesis technique, its advantages over the conventional methods and the principles thereof. Effects of γ-irradiation and the conditions required for the structural modification of graphene to obtain different graphene composites are detailed. The influence of operational parameters on the fabricated graphene-based composites are discussed followed by summaries of recent developments in the applicability of γ-irradiated GBNMs in catalysis, energy, sensing, and biomedical fields. In addition, this paper presents insights into the challenges posed and provides future research directions and prospects in the field of γ-irradiated GBNMs.

Introduction

Graphene is a largely studied nanomaterial that has drawn tremendous interest from basic research and industrial sectors owing to its properties that are reliant on its inherent structure [1]. Graphene refers to a monolayer or bilayer graphene sheet [2]. It is made up of carbon (C), with a $1s^2$ $2s^2$ $2Px^1$ $2Py^1$ $2Pz^0$ ground state electronic structure. Since the energy level of 2pz is empty but equal to the energy levels of 2px and 2py, the carbon's valence shell electrons can form three types of hybridization known as sp, sp^2 and sp^3. One C atom shares sp^2 electrons with three other neighbouring C atoms forming an atom thick two-dimensional (2D) honeycomb planar structure. These are essentially in-plane σ bonds created by the hybridized orbitals of sp^2 (2s, 2px, and 2py), while the 2pz orbitals, which are perpendicular to the planar

* Corresponding authors at: UNESCO-UNISA Africa Chair in Nanosciences & Nanotechnology Laboratory, College of Graduate Studies, University of South Africa, Muckleneuk Ridge, P.O. Box 392, Pretoria 0002, South Africa (F.T. Thema).
E-mail addresses: azizis@unisa.ac.za (S. Azizi), ftthema@gmail.com (F.T. Thema).

https://doi.org/10.1016/j.flatc.2024.100662
Received 16 January 2024; Received in revised form 10 April 2024; Accepted 18 April 2024
Available online 21 April 2024

structure, establishes σ bonds with the two nearby out-of-plane C atoms. The resultant covalent σ bond in monolayer graphene has extraordinary mechanical capabilities due to its short interatomic length of approximately 1.42 Å, making it even stronger than the sp^3 hybridized carbon–carbon bonds found in diamonds. The half-filled π band allows free movement of electrons thus giving a conduction feature to graphene. This band also forms the conduction and valence bands with zero band gap [3]. Other salient properties of graphene include flexibility, high light absorption and transmission, heat resistance, and environmental friendliness [4]. The electronic properties are determined by the number of graphene sheets [3]. Owing to peculiar properties of graphene there has been a plethora of research on the application of graphene and graphene composites in catalysis [5], electrodes [6], energy storage [7], adsorption [8] and sensors [9] among others. The challenge however is that the acquirement of graphene nanosheets as raw material is both difficult and costly. Using the scotch-tape approach, graphene was generated by micromechanically cleaving highly ordered pyrolytic graphite, however the product yield was very low [10]. Ritter and Lyding realized mono and bilayers of graphene via the mechanical exfoliation technique [11], which also suffer from low throughput thus limiting large-scale production. Among the popular methods of producing graphene, reduction of GO is prominent because it doesn't require complicated equipment [12].

GO is mostly produced via the oxidation of graphite using either the original or the modified Hummers method [13] in the presence of strong and very concentrated acids and oxidants. The resultant GO sheets are separated to individual layers by ultrasonication. Although the hybridization in graphene is sp^2, during oxidation of graphite to GO, the 2s electron gets excited to the 2pz orbital creating free π electron in excited state. The oxygen atoms are attached to the free π electron (pz electron) and forms C-O bonds in graphite layers and converts sp^2 to sp^3 hybridization and create defects that reduce the electrical conductivity of the material [14]. The oxygen containing moieties, OH and C-O-C on the surface of the sheets and COOH at the edges of graphene confer GO with hydrophilicity as such it can dissolve in water and disperse in several organic solvents. Moreover, the oxygenated groups serve as centres of covalent functionalization of GO with other functional groups to improve or alter its properties to suit certain applications. The electrostatic, π-π and Van der Waals interactions which are week interactions take part during non-covalent bonding of GO with target molecules [15]. To restore the electrical and mechanical properties, GO must be reverted to graphene via reduction techniques to form reduced graphene oxide (rGO) before or during its conversion to generate other GBNMs that comprise zero-dimensional (0D) quantum dots, and 3D hydrogels and aerogels.

Although the produced GBNMs are widely applicable, there exist a need to improve their structural properties to enhance their application efficiency in the various fields. This is often achieved by inducing surface defects such as point defects (0D), line defects (1D), planar defects (2D), and volume defects (3D) in a controlled manner. Therefore syntheses methods that yield to satisfactory reduced graphene with desired surface defects or vacancies are being explored [16]. The chemical reduction method is commonly used; however, the produced graphene suffers from incomplete reduction and defected carbons thus compromising the properties of rGO. Moreover, this method requires the use of high temperatures, toxic precursors and long processing time among others [17]. While thermal techniques efficiently reduce GO [18], there are few appropriate substrates, the process is energy demanding, and pose a serious threat to safety [19]. Like chemical syntheses methods, low temperature hydrothermal approaches produce incompletely reduced GO. Mechanical exfoliation on the other hand achieves good quality graphene but generates undesired structural defects, uncontrolled morphologies and multiple layered GBNMs. Due to the mentioned drawbacks encountered by conventional GO reduction/modification methods, focus has been directed to greener alternatives i.e. using plant extracts [20], photothermal [21], and electrochemical reduction [22]. Although these environmentally friendly approaches can be utilized to produce graphene composites, they also need precise synthesis conditions and are lengthy [23].

Among the many alternative approaches for preparing GBNMs in recent years are the radiation techniques that can either be non-ionizing or ionizing. Non-ionizing radiation comprise microwave [24,25], laser [26], infrared [21] and ultraviolet [27], among others. Ionizing radiation on the other hand encompass the use of X-rays and the γ-rays of which γ-rays have the highest energy. Generally, all the irradiation processes offer a facile, and scalable approach to produce high-quality graphene materials. The advantages of modifying GO using the irradiation approaches are; the production of products with minimal waste [28], low energy demand therefore sustainable, and the applicability of wide variety substrates [29]. These techniques also produce high purity graphene and enables the user to control the irradiation times and dosages/intensities thus avoiding aggregation of graphene sheets which is one of the key stumbling blocks hindering the production of rGO at industrial scale [30]. Since graphene is a good absorber of radiation [24], radiation energy induce various chemical reactions, including synthesis, reduction, exfoliation, doping, functionalization [31], and generation of novel graphene-based composites such as graphene-metals/metal oxides etc [32].

In the case of ionizing radiation *viz* γ-rays, the high energy irradiation interacts and imparts energy to samples and cause either a gain or loss of electrons and hence ionization of the material [33]. Like in the case of non-ionizing radiation (microwave) γ-radiation energy also creates vacancies, defects, and dislocations in graphene materials, resulting in modification of the electrical, optical, and physical properties [34,35]. Since γ-rays exhibit maximum energy with longer penetrating capability into materials due to its zero charge and mass, the γ-modified GO samples are entirely reduced in depth over and above the other advantages of radiation techniques in general [36,37], as a result there are a handful reports available on the use of γ-irradiation to prepare graphene and its derivatives for different applications [28].

While there are plenty review articles detailing other irradiation methods, there are only few available reviews on γ-radiation induced synthesis of nanomaterials. Not only are they few these are on syntheses of metallic nanoclusters [38,39] and polymer nano-composites [40] not GBNMs. While, Tung et al. [29] recently reviewed the irradiation methods including the γ-radiolysis technique for engineering GBNMs collectively, based on our knowledge there is no published review focusing solely on the γ-irradiation of GBNMs to explore the effect of this radiation technique on their structure in relation to their application. Therefore, this review aims to introduce graphene and highlights conventional techniques for obtaining graphene derivatives and their drawbacks prior to discussing the modern radiation techniques under which γ-radiation is categorised. The advantages and principles of γ-radiation assisted synthesis are elucidated before the different constructs of graphene comprising of reduced GO, etched graphene, graphene/metal/metal oxides and functionalised graphene composites achieved with the aid of γ-radiation are presented. Furthermore, the factors that influence the modification of graphene composites are presented. In light of this, recent progress in the usage of γ-radiation synthesized GBNMs in photocatalysis, energy storage, sensors, antimicrobial activity, and cancer treatment were summarized. In addition, the challenges faced during the production of GBNMs by γ-irradiation, research directions to circumvent these challenges, as well as prospects in this area are provided.

The principles of γ-irradiation

Since γ-rays' photons are highly energetic with a deeper penetrating power in water they directly interact with materials through processes like pair formation, the photoelectric effect, and Compton scattering [41]. The two commonly used γ-irradiation sources are cobalt-60 (^{60}Co) and cesium-137 (^{137}Cs) that discharge photons to create secondary

electrons, which contribute in the formation of ions and free radicals, among other products [38]. ^{60}Co is however the most frequently used due to its extended half-life and emission of 1.25 MeV compared to ^{137}Cs that emits γ-rays of only 0.66 MeV. The amount of radiation absorbed by the samples from the source is known as the total absorbed dose and its unit is Gray (Gy or kGy). Since the Gray is based on the dose rate whose units are (kGy/h or Gy/min), the D is obtained by regulating the radiation exposure time "t" of the sample of interest.

When exposed to γ-rays, the molecules in the aqueous media or powder samples ionize, which is followed by electronic excitation that produces large amounts of reactive species that are uniformly distributed within the sample [42]. The primary reaction species are, aqueous electrons (e^-_{aq}), hydrogen radicals (H·), hydroxyl radicals (OH·), hydrogen gas (H_2), hydrogen peroxide (H_2O_2) and other radiolysis species [43]. The e^-_{aq}, H· and H_2 are reducing agents while the $OH^{\cdot}$, $H_2O^{\cdot}$, H_2O_2, and $O_2^{\cdot}$ serve as oxidizing agents [44]. The concentration of the reactive species (Eq. (1) progressively approaches a pseudo-equilibrium state under continued radiation in an aqueous environment. Fig. 1 depicts the 3 phases of γ-radiolysis of water: the physical phase, the physicochemical phase, and the non-homogeneous chemical phase [42].

Depending on the desired modification on the GBNMs, either the reducing or oxidizing agents are introduced into the reaction vessel. When reducing environments are required alcohol is frequently introduced in the water medium to generate alcohol radicals that scavenge the oxidants produced by water. The alcohol radicals are generated via hydrogen abstraction as shown in the in Eq (2) and (3) [45]. In some cases, alcohol or water-alcohol medium is replaced by solvents like N,N dimethylformamide (DMF) [28] and ethylenediamine (EDA) [46] that also serve as scavengers of oxidative radicals. The samples are then irradiated under inert conditions or oxygen, hydrogen, etc conditions as informed by the desired modification as discussed in later sections. Alternatively, dry sample materials (GBNMs) are radiated where gases such hydrogen and others replace the aqueous medium. The gases prevent aggregation of the formed rGO observed in suspensions. In this approach, the incident γ-rays splits hydrogen into radicals that attacks the surface groups of GO (Fig. 1b).

$$H_2O^{\gamma-\text{radiolysis}} \rightarrow e^-_{aq},\ H_3O^+,\ H,\ H_2,\ OH^{\bullet}, H_2O_2,\ OH_2 \quad (1)$$

$$(CH_3)_2\,CHOH + HO^{\bullet} \xrightarrow{k_{p1}} (CH_3)_2\dot{C}OH + \dot{C}H_2CH(CH_3)\,OH + H_2O$$

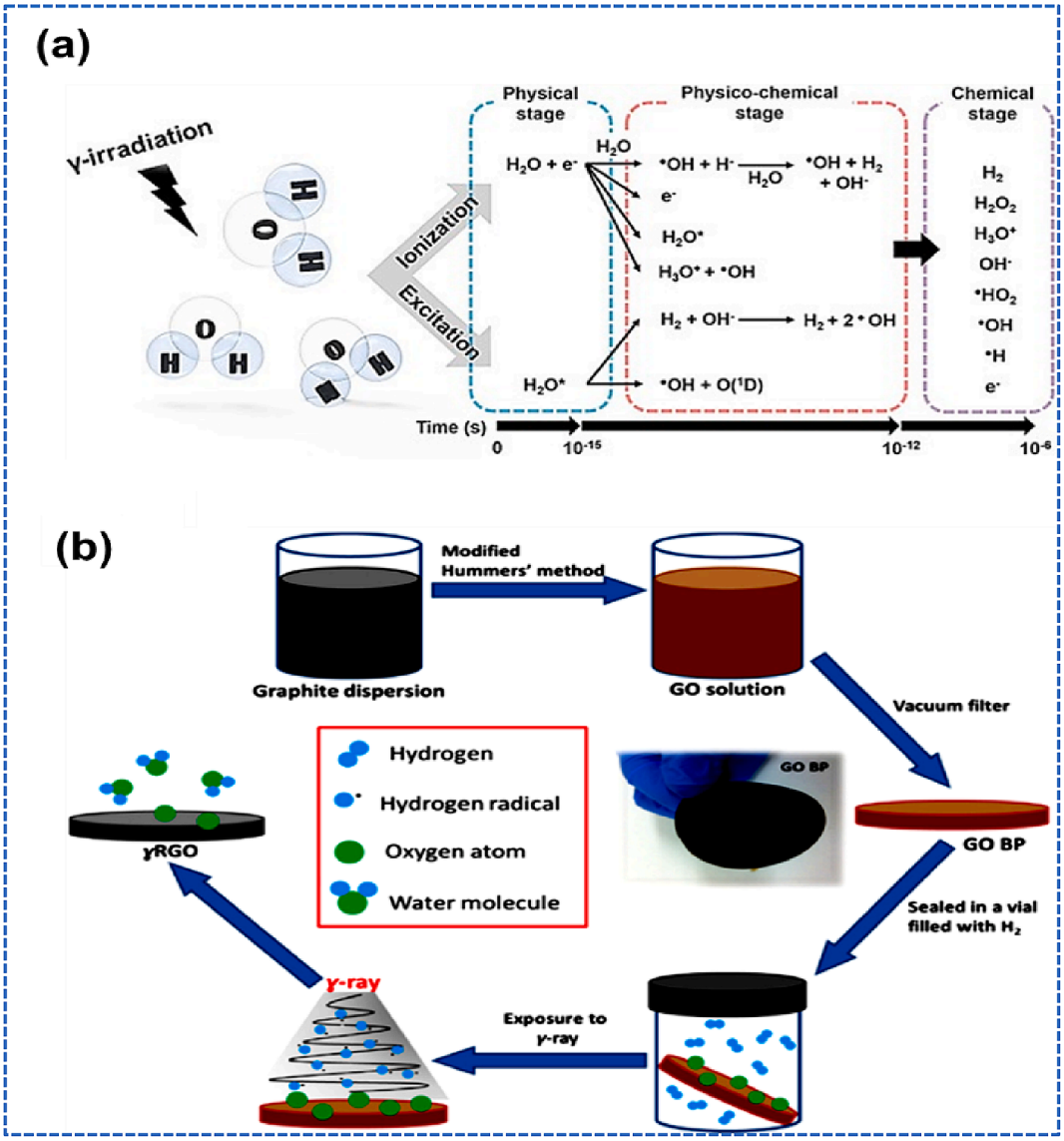

Fig. 1. (a) Schematic diagram showing generated reactive species at different stages as a result of ionization of water by γ-radiolysis in water–ethanol medium. Reprinted with permission from ref. [38]. (b) γ-ray reduction of dry GO Bucky papers (GO BP) in the presence of hydrogen gas (dry reduction). Reprinted with permission from ref. [47].

$k_{p1} : 1.9 \times 10^{9} Lmol^{-1}s^{-1}$) (2)

$CH_3CHOH + H\bullet \xrightarrow{k_{p2}} (CH_3)_2\dot{C}OH + H_2 (k_{p2} : 7.4 \times 10^{7} Lmol^{-1}s^{-1})$ (3)

Modification of graphene based nanomaterials (GBNMs) using γ-irradiation

γ- irradiation can be applied for different purposes on GBNMs. The technique can be used to etch, reduce, or functionalize graphene composites. The following sections point out to the various modifications achieved through γ- irradiation in GBNMs.

Etching of GO using γ- irradiation

Since porous graphene sheets possess large surface area, adjustable porosity, and high densities of unsaturated carbon edges surrounding the pores, they are appealing candidates for applications such as catalysis, energy storage, separation, and sensing. There are several published methods for perforating graphene, such as etching, controlled growth mechanisms, of which the use of γ-radiation is one of them [48].

As previously mentioned, γ-irradiation of water, produces $OH^{\bullet}$ and e^{-}_{aq} as the major oxidative and reductive agents respectively, the oxidation the GO sheets could possibly occur in three different ways; (i) the $OH^{\bullet}$ can either transfer an electron to GO, (ii) extract H-atom from GO, and (iii) hydroxylate GO by adding to the C = C bonds of the GO [49]. For instance, when nitrous oxide (N_2O) was irradiated in a saturated GO solution, the $OH^{\bullet}$ radicals occupied the sites that were previously occupied by oxygen functional groups to form hydroxylated radicals. The formed hydroxylated radicals went through ring opening, while the C atoms bonded to the oxygenated groups were oxidized and eliminated as CO_2 or CO, resulting to the development of C vacancies on the GO layers. The $OH^{\bullet}$ radicals attach next to the formed vacancies since these sites are chemically active compared to those within the conjugated network. As the oxidation process progresses the carbon vacancies grow into nano-scaled defects making the sheet porous or channelled as shown in Fig. 2a [49]. In another study, the edges and planes of graphene were etched by adding GO in a solution of styrene and toluene (1:1 vol ratio) prior to γ-irradiation at a total absorbed dose of 200 kGy and a dose rate of 2.0 kGy/h under ambient conditions [50]. Luvodic and colleagues simultaneously reduced and perforated GO to produce porous rGO sheets with narrow pore size (3 nm) distribution and large surface pore density by exposing the GO under γ-ray (100–500 kGy) irradiation in the presence of hydrogen without additional chemicals

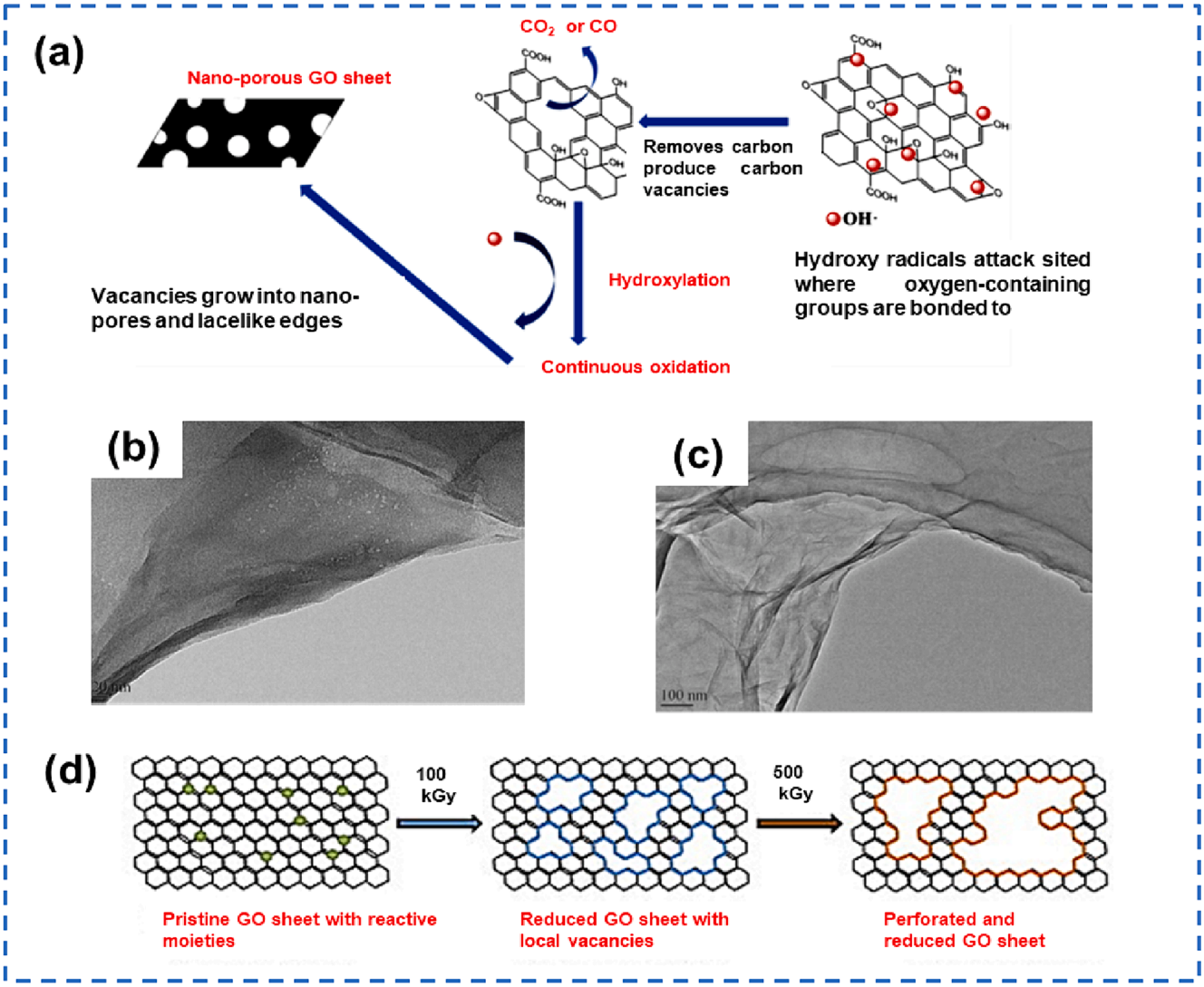

Fig. 2. (a) The mechanism of etching of GO using γ-irradiation where oxidized carbon is eliminated as carbon monoxide or carbon dioxide. Reprinted with permission from ref. [49], (b) TEM image of pristine GO sheet, (c) GO irradiated at 500 kGy. (d) pathway of perforation in rGO with the increase in the γ-radiation total dose. Reprinted with permission from ref. [51].

(Fig. 2b). The etched rGO's morphology was similar to that of the nascent GO (Fig. 2c) as in the case of chemically reduced samples. Like previously reported findings, the mechanism for pore formation entailed reduction and creation of vacancies at low dosage followed by etching of the vacancies to form well defined pores at higher dosages as indicated in Fig. 2d [51]. In a unique study GO membranes with short-range pore channels were fabricated via γ-ray etching. The radiated GO membrane exhibited numerous short-range in-plane pore channels that formed because of defect formation. The in-plane porosity and expanded interlayer pathway were finely tuned by controlling the irradiation dose. These short channels reduced the mass transfer pathway for the migration of water molecules and hence elevated water permeability (345.23 L $m^{-2}h^{-1}$ bar^{-1}), dye rejection (~100 %) and an enhanced dye/salt separation. All these values were superior to GO membranes previously reported [52].

Reduction of GO by γ-radiation

The synthesis of GO that is later reduced to make graphene is easier compared to direct preparation graphene from graphite. However, the electrical properties of GO are poorer than that of graphene attributed to the prevalence of oxygen-containing functional groups that result in more sp^3 instead of sp^2 hybridization therefore these oxygen must be removed from GO (reduction) [53]. Reduction of GO is basically the elimination of the OH and C-O-C the surface and COOH groups from the edges of GO followed by annealing the intrinsic defects to enhance the electrical properties of GO [54]. As mentioned in section 1, the reduction of GO can be obtained via conventional techniques which however suffer from drawbacks. The γ-irradiation technique reduces GO in the presence of antioxidants or oxidant scavengers (alcohols) and other polar aprotic solvents. The antioxidants hinder the oxidative radicals from further oxidizing the GO [55]. The absence of oxygen is ensured further by bubbling the medium to be radiated with inert gases (Ar or N_2).

During the reduction experiments, e^-_{aq} is the most active reductant with a redox potential of E° (e^-_{aq}) = − 2.87 V_{NHE} at pH 7 followed by $H^\bullet$ with a redox potential of E° ($H^\bullet$) = − 2.3 V_{NHE}) [38]. The interactions between reductive species and oxygen-containing functional groups lead to the removal of oxygenated groups, promoting the reconstruction of π-π conjugation and hydrogen bonds [46]. The π-π conjugation arise from the hydrophobic nature of graphite and is assessed via the degree of reduction of rGO nanosheets. Hydrogen bonding is formed between single bonds of COOH and OH on the unreduced segments of GO and molecules of the polar solvent [45]. The advantages of γ-radiolysis assisted reduction over conventional methods are as follows: (i) reduction occurs in the absence of extra reductants and thus prevents the production of undesired products, (ii) reducing species are uniformly dispersed in the solvent, (iii) energy is absorbed irrespective of the existence of light-absorbing substances, (iv) a facile and cost-effective technique and (vi) ease of size, shape and size distribution control of the nanomaterials by optimizing the total absorbed dose and dose rate [41].

The first account of γ-radiation induced reduction of GO to form rGO was reported by [56] in a water-alcohol medium. After irradiating the sample with 35.3 kGy, the GO's dispersion colour changed from yellowish brown to black. The reduction was confirmed by the UV–Vis spectra where the peak of GO cantered at 290 nm due to the n → π* conversion of C = O bonds disappeared while the strong absorption peak at 230 nm due to π → π transitions of aromatic C–C bonds red-shifted to 270 nm [56]. In another study GO was exfoliated in distilled water via sonication prior to adding ethanol and subsequent irradiation with doses of 20, 40, and 80 kGy respectively at (2 kGy/h). These were labelled γ-rGO. In a separate experiment GO was reduced chemically using hydrazine (H-rGO). The γ-rGO had a higher thermal stability than H-rGO, an indication that γ-rays are effective in removing thermally unstable oxygen groups on GO surfaces [57]. Well-dispersed graphene sheets were also obtained by dissolving GO in DMF at room temperature. After sonicating and bubbling the mixture with N_2 it was exposed to 300 kGy at 300 Gy/min. The resultant rGO displayed enhanced mechanical stability because of the anchoring of $N(CH_3)_2^+$molecules on γ-rGO [58]. DMF served as a reduction medium in another study where the dose rate was reduced to ~ 45 Gy/min to achieve 15 kGy. The obtained rGO had no observable defects and aggregation [28].

Due to the penetration ability of γ-rays the technique is applicable for fabricating 3D rGO aerogels and hydrogels regardless of their size and thickness. The first report on synthesis of 3D aerogels via γ-irradiation in a water-isopropanol medium was documented by [44]. The same group prepared another rGO aerogel by dispersing GO in a mixture of EDA and water followed by γ-ray irradiation. Like alcohols, EDA served as the radical scavenger thereby encouraging reduction and self-assembly of the formed rGO (Fig. 3a). The rGO aerogel's surface was smooth with wrinkles (Fig. 3b) and its hydrophobicity was confirmed by the 122° contact angle (Insert, Fig. 3b). The cross section of rGO aerogels exhibited hexagonal 3D porous structure with narrow passages and walls that were assembled due to piling of rGO nanosheets (Fig. 3c) [46]. The EDA molecules participated in either nucleophilic ring opening of epoxy groups or condensation reaction with carboxyl groups on the surface of GO as depicted in Fig. 3 (d1 and d2). The e^-_{aq} potentially attached to carboxyl groups (Fig. 3d3) or broke the epoxy bridges to encourage the formation of O–H and C–H bonds as shown in Fig. 3d1. Alternatively, the e^-_{aq} abstracted the O–H group to form C = C as illustrated in Fig. 3d4. Briefly, the EDA radicals eliminated the oxygen-containing groups, restored the conjugation of C = C and bound on the GO surfaces.

The reduction of GO using whole plants or plant extracts has captured the interest of numerous researchers, particularly for biomedical applications due to the biocompatibility conferred by the functional groups of phytochemicals. Therefore, chemical scavengers of oxidative free radicals were substituted with natural antioxidants found in ginger, aloe vera, and a mixture of ginger and aloe vera to make ginger (G-rGO), aloe vera (A-rGO), and aloe vera/ginger (AG-rGO) respectively under γ-irradiation with 80 kGy of at 1 kGy/h. The XPS revealed that the intensity of the C–C peak improved from 0.50 for GO to 1.35, 1.25, and 1.43 for G-rGO, A-rGO, and AG-rGO, respectively in comparison to the C–O peak indicating an enhanced ratio of sp^2 which is a validation of reduction process [59]. In a separate study, γ-radiolysis of GO solution containing *Hyphaene thebaica* fruit powder instead of chemical scavengers was reported by Taha and colleagues. The Fourier transform infrared spectroscopy (FTIR) confirmed the removal of most oxygen functional groups from GO and conjugation between *H. thebaica* and the rGO. Furthermore, the High-Resolution Transmission Electron Microscope (HRTEM) showed smooth and transparent sheets of GO with few crinkles while the rGO exhibited a more crinkled morphology and folded appearance [60].

Functionalization of graphene with the aid of γ-ray radiation

Functionalization of the graphene's surface is a crucial step to enabling its applicability since nascent graphene is inactive and thus displaying poor chemical activity and solubility in water. With the presence of functional groups on their surfaces, GO and rGO can further be functionalized to improve their physicochemical properties. Guo et al. [61] categorized graphene functionalization strategies into covalent [62], non-covalent [63], plasma hydrogenation [64] and nanoparticle functionalization [65]. The limitations of these fonctionnalization techniques comprise of the involvement of toxic reagents, lengthy reaction duration, specific reaction conditions thar hinder large commercialization among many. These issues need the development of innovative ways for functionalizing graphene that combine the advantages of chemical synthesis with economic benefits

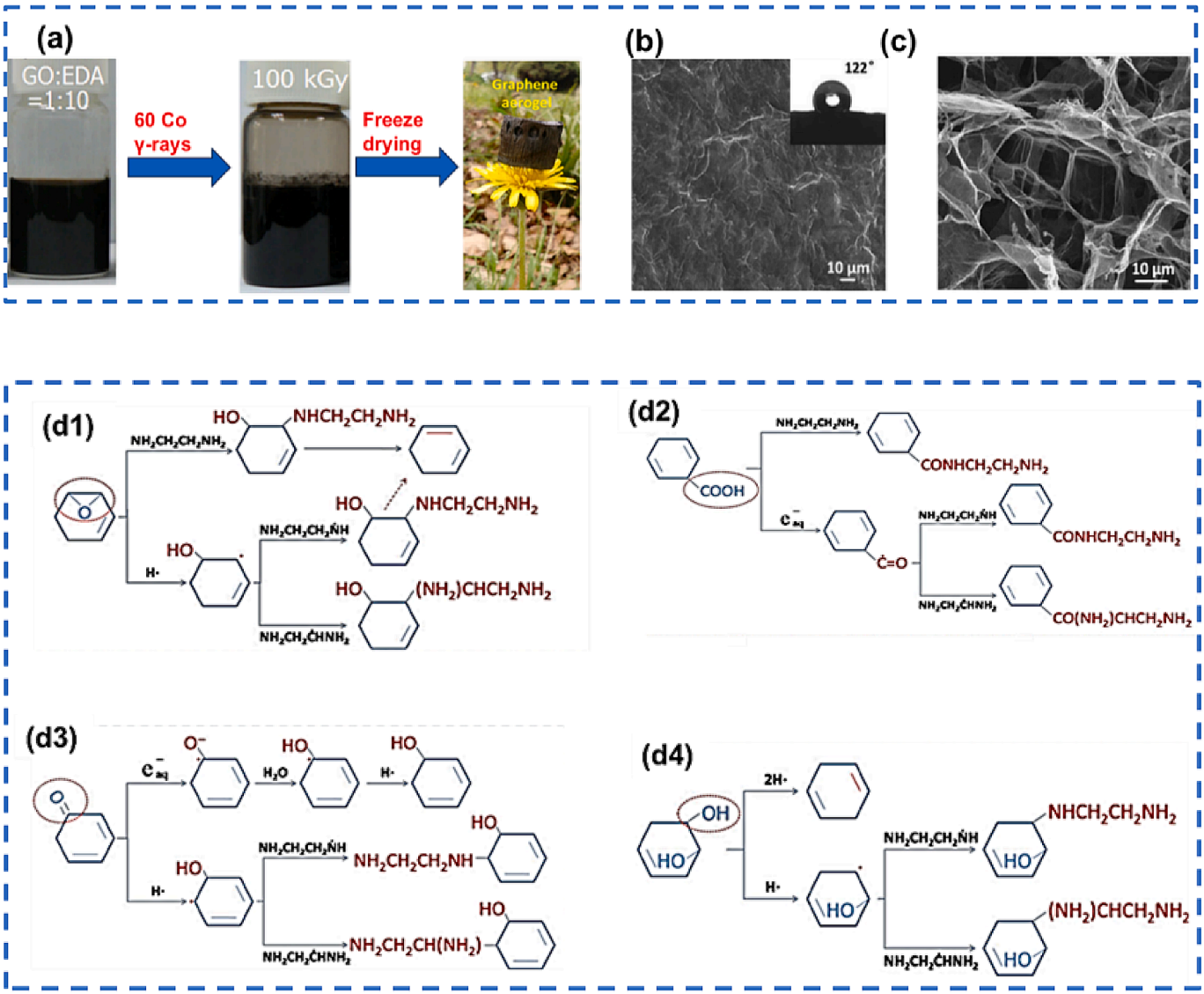

Fig. 3. (a) Schematic diagram for the synthesis of rGO aerogel via γ-ray irradiation in a water–ethanol medium at room temperature, (b) SEM micrographs of the surface and (c) cross-sectional of rGO aerogel, (d1-d4) Possible reaction mechanisms between GO and EDA during γ-ray irradiation. Reprinted with permission from ref. [46].

while demonstrating improved reduction efficiency. Currently, only few researchers have investigated the use of γ-ray radiation as an alternate method for modifying graphene's physiochemical characteristics.

A milder γ-ray induced grafting method for surface functionalization of GO with octavinyl polyhedral oligomeric silsesquioxane (OvPOSS) was demonstrated for the first time. The grafting improved the thermal stability and increased the interlayer distance thus improving the reactivity of GO. Increasing the dose to 50 kGy resulted into a superhydrophilic GO due to incorporation of N containing group on the composite's C = C matrix. The XPS showed the presence of the Si 2p and Si 2s peaks in the spectrum of functionalized GO, a confirmation of OvPOSS's attachment on GO [66]. In another study, aqueous solution of exfoliated GO was added into a solution of octadecylamine, dodecylamine, and tetradecylamine in ethanol respectively. The solutions were exposed to 25 kGy to functionalize the GO with alkyl chains. The FTIR showed (–CH_2) absorbance peaks at 2960–2850 cm^{-1} originating from alkyl chains. In addition, there was a peak in the region 1560–1450 cm^{-1} that confirmed the presence of C–N and H–C bonds. Moreover, the modified GO also possessed enhanced thermal stability [67]. Organosilane modified GO sheets were achieved by grafting 3-aminopropyltriethoxysilane (APTES) and 3-glycidyloxypropyltrimethoxysilane (GPTES) on GO via γ-ionization with 50 kGy, 100 kGy and 150 kGy doses respectively. An increase in the I_D/I_G ratio was observed with the increase in the absorbed dose in the Raman spectra. This suggested that an increase in the the radiation dose, increased the silane content in functionalized GO and led to creation of more defects [68].

Doping of graphene using the γ-radiation technique

The applicability of graphene is hindered by its intrinsically hydrophobic nature and lack specific active sites [69]. GO, a graphene derivative on the other hand contains oxygen-containing groups that are sp^3 hybridized. Even though the sp^3 domains create defects and enlarge the band gap, making GO a poor electrical conductor [70], the advantage that comes with the oxygen-containing groups is that they are easily modified by physical and chemical processing, making GO a suitable precursor for doped graphene [71]. Doping refers to the introduction of atoms such as B, N, P, S, or metal/metal oxide (MO) clusters into the carbon matrix of graphene derivatives [72]. This process improves the materials electrical properties, mechanical stability and semiconducting

nature. Doping graphene with non-metals converts the material's surface from non-polar to polar because of their differing electronegativities to C atoms. N is the most favourable element because its atomic size is comparable to that of C. Moreover, it has five valence electrons that form a strong C − N covalent bond [73]. The presence of N in the carbon matrix of graphene results to strong electron withdrawal from C whose electronegativity is 2.44 to N with a higher electronegativity (3.4).The C therefore carries a positive charge density which becomes the centre of attractive forces [74]. Moreover, the insertion of atoms results in widening of graphene's energy band gap (E_g). In the case of B, because the size of B and its valence electrons are almost similar to those of C, the only observed change in the lattice parameter of graphene is a slightly longer bond length of the B-C compared to C–C in the graphene lattice. Like B, the electronegativity of S is very close to that of C therefore minor polarization of the C-S bonds is noticeable, so, the defective sites in graphene are caused by the bigger bond length of the C–S bond as compared to the C–C bond. In comparison to N, P-doping causes more structural damage due to its larger size [70]. The choice of dopants therefore is influenced by the working mechanism of the intended device and its application.

N-doping of graphene is more favourable and literature has proven that it has beneficial effect on its properties such as surface area, pore size distribution, and electrical conductivity, that enhance the applicability of graphene in energy storage devices for example [75]. Thus, facile, and high yield producing doping techniques are studied. Classical methods for doping graphene include chemical vapour deposition [76], arc discharge [77], N_2 plasma treatment [78] all of which are limited by the requirement of complex instrumentation and low yield. Heat treatment techniques like gas annealing and pyrolysis are limited by long time and high temperature synthesis apart from giving a low yield [79]. Solvothermal processes require the usage of toxic solvents [80]. The advantage of the γ-radiation method in this regard is that it triggers an interaction between the carbon matrixes of graphene and the N source eliminating the need for toxic solvents and high temperatures [81,82]. As such, 4 wt% N was inserted into graphene using ethylamine as a nitrogen source via γ-irradiation at 30 kGy via the dry method. The graphene and the ethylamine were placed in separate open test tubes. These were then enclosed together in one sealed transparent box that was inserted in a γ-radiation chamber followed by irradiation whereas the wet method led to only 2 wt% N-doping in the graphene plates [81]. Recently, γ-radiolysis has been employed in the preparation of N-doped rGO-supported iron (Fe)-based catalysts, where the wt.% of Fe loading varied from 10 to 20 %. A mixture of powder rGO and urea was prepared at a 3:1 mass ratio and dispersed into a water–ethanol that contained various amounts of iron (III) nitrate. After sonication and deoxygenation the samples were irradiated at 100 kGy (2 kGy/h). The obtained composite was used as an oxygen reduction reaction catalyst [82].

Graphene composites prepared via γ-radiolysis

Composite materials are made up of two or more materials with substantially diverse physical and chemical characteristics that, when combined, result in a material with unique properties from each individual component [83]. Owing to its salient qualities, graphene has been coupled with metals [84], metal oxides [85] and polymers [86] among many to form composites to either improve the properties of graphene or vice versa. This section is dedicated to discussing graphene composites that were prepared via the γ-radiosynthesis method.

Graphene-metal composites prepared by γ-radiosynthesis

Metal nanoparticles (MNP) and their nanocomposites are widely utilized due to their diverse applications. One of the challenges in the synthesis of MNP is agglomeration because of Ostwald ripening, a process that increases the size distribution of the as-prepared MNP. Also, while MNPs possess large carrier density their drawback is the limited carrier mobility. Graphene on the other hand is also prone to aggregation but unlike MNPs has exceptional carrier mobility but suffers from small carrier density [87]. To curb the challenge of agglomeration in MNPs, scientist synthesize metallic nanomaterials on suitable supports of which graphene is regarded as one of the best. As a support material graphene serves to control the MNP's shape and size, inhibit agglomeration, and absorb metal ions to simplify the reduction of MNPs [88]. The synergistic properties that evolve from graphene/metal hybrid structures are beneficial to different applications [73] due to the trade-off between carrier mobility in graphene and carrier density in NMPs that brings about composites endowed with high electron mobility and electron density [87]. Even though the graphene-MNP nanocomposites display enhanced properties (conductivity) and selectivity, it is difficult to deposit uniform MNP onto graphene because of its poor chemical reactivity and interfacial free energy [61]. The γ-radiosynthesis method is an excellent approach for producing graphene-MNPs since it homogenously and instantaneously produce metallic nuclei with a narrow particle size distribution and uniformly dispersed MNPs on the surface of graphene. Graphene-NMPs composites that have been fabricated with the aid of γ-radiosynthesis are discussed in the following sections.

Graphene-silver. Silver nanoparticles (AgNPs) supported on GO were obtained by introducing pre-prepared imidazole silver nitrate (Ag$(im)_2NO_3$) into a mixture of GO, polyvinyl-pyrrolidone (PVP) as a stabilizing agent and isopropanol (IPA) as the oxidant scavenger. The mixture was then γ-irradiated at 150 kGy. GO was intercalated by the Ag$(im)_2NO_3$ and the AgNPs between the sheets of GO were reduced and grown as illustrated by schematic in Fig. 4a. The size of AgNPs was determined by the conformation effect of GO while PVP ensured monodispersed and spherical shaped AgNPs. In the absence of PVP (Fig. 4b) the NPs exhibited a variety of shapes with a broader size distribution whereas in the presence of 0.5 % PVP the NPs are spherical with a narrow size distribution (Fig. 4c). The XRD indicated that the addition of PVP enhanced the peak intensity ratio of Ag(1 1 1) to Ag(2 0 0) which are crucial for the size and shape control of nanocomposites [89]. A separate study demonstrated that GO also acts as a radical scavenger to promote reduction and growth of MNPs. An aqueous mixture of GO, $AgNO_3$, $HAuCl_4{\cdot}4H_2O$ and $H_2PtCl_6{\cdot}6H_2O$ was prepared. After being purged with Ar, the suspensions were irradiated with absorbed doses of 150 KGy (2.7 kGy/h). The resultant Ag/Au/Pt-GO composites were pure and well dispersed, an indication that the oxygen-containing moieties on GO can be converted to reducing agents that reduce both the MNP and GO simultaneously while promoting and controlling the growth of MNPs [90].

Graphene-Platinum. Simultaneous reduction of graphene and generation of PtNPs was achieved by preparing aqueous solutions of GO with appropriate amounts of graphene and Pt (IV) using sodium dodecyl sulfate (SDS) or IPA respectively. The mixtures were purged with Ar, ultrasonicated and irradiated at ambient conditions with γ-rays at 15 kGy/h for 40 min. The two products were labelled Pt/graphene-SDS and Pt/graphene-IPA, respectively. The TEM images of Pt/graphene-SDS and Pt/graphene-IPA reveal uniformly dispersed PtNPs on graphene as shown in Fig. 4(d-e) respectively. Smaller PtNPs (15 ± 4.0 nm) with narrower size distribution were formed in IPA (Fig. 4f) than those in SDS (29 ± 7.8 nm) (Fig. 4g). The group proposed two possible mechanisms for formation of graphene/Pt composites. The less likely mechanism is depicted in Fig. 4h where graphene in the aqueous phase hypothetically interacts with $OH^{\bullet}$ in the beginning of reactions, followed by the formation of carbonyl groups on graphene. The Pt precursor ions then attach to the formed adsorption sites by electrostatic interaction before the radiolytic reduction of Pt and subsequent growth of PtNPs on graphene. The most likely reaction mechanism is that Pt ions are reduced to NPs in the bulk solution before electrostatically attaching to the reduced graphene as displayed in Fig. 4i [84].

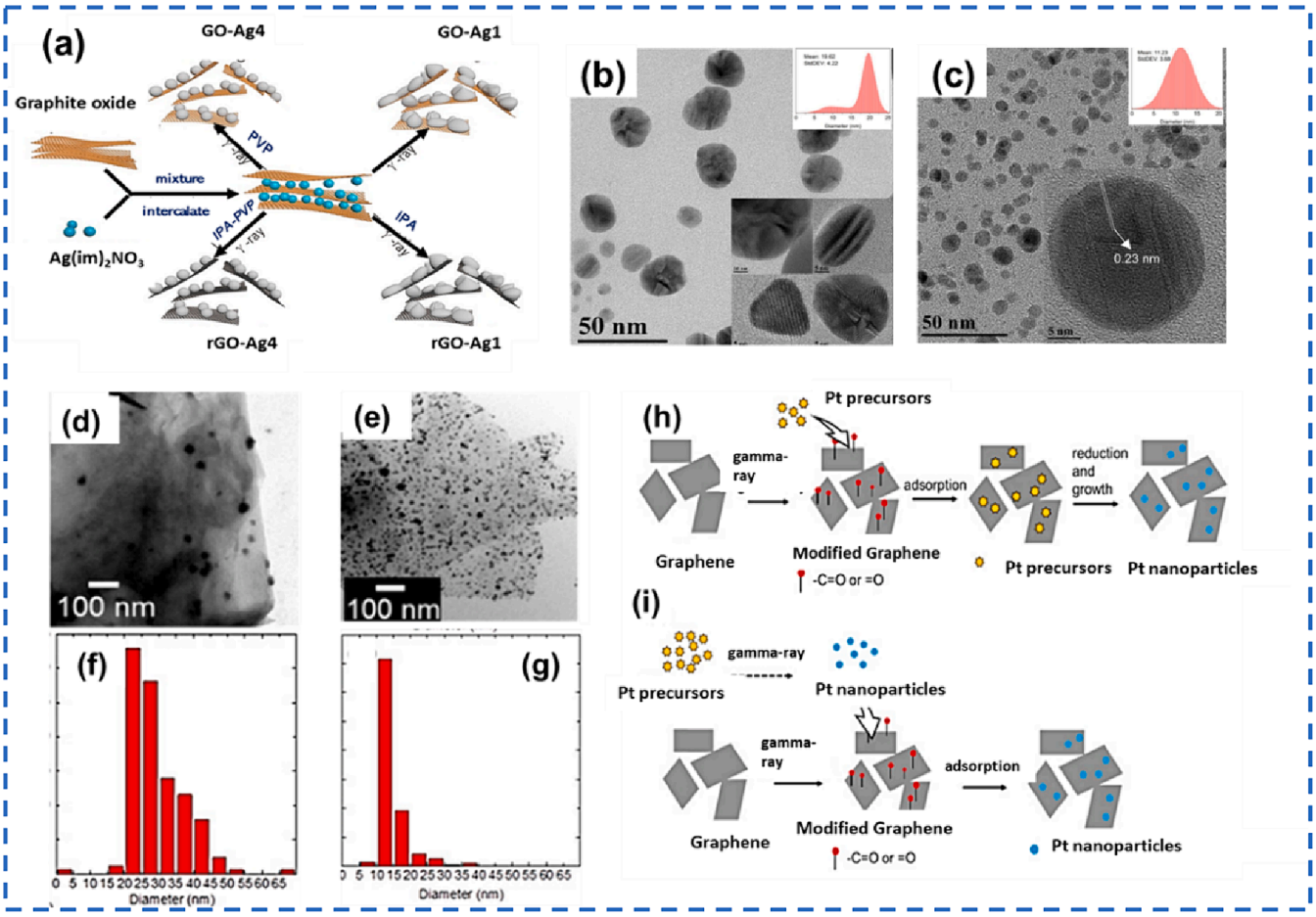

Fig. 4. (a) Schematic for γ-irradiation of graphene-AgNPs without PVP or IPA (GO-Ag1), in the presence of PVP (GO-Ag4), in the presence of IPA (rGO-Ag1), and in the presence of both PVP and IPA (rGO-Ag1), HRTEM images of (b) pristine graphene-AgNPs in the absence of PVP and (c) graphene-AgNPs in 0.5 % PVP. Reprinted with permission from ref. [89]. TEM micrographs of (d) Pt/graphene-SDS, (e) Pt/graphene-IPA, (f) size distribution Pt/graphene-SDS, (g) Pt/graphene-IPA, Possible mechanisms of graphene-Pt formation (h) less likely, and (i) most likely. Reprinted with permission from ref. [84].

Graphene-Gold. Electrochemically exfoliated graphene was employed to anchor gold NPs (AuNPs) prepared via the reduction of chloroauric acid under γ-irradiation at low doses (1,5 and10 kGy) without reductants and stabilizers. Increasing the dose reduced the size of the as-synthesized AuNPs. At all the doses five morphologies were attained, namely hexagonal, spherical, triangular, rod-shaped and trapezoidal with size ranging between 11 and 20 nm. Due to the hydrophilic nature of graphene, the graphene-Au composites were endowed with long term stability [91]. Another group suspended Au^{3+} and GO in a water–ethanol medium. The reactants were instantaneously reduced and self-assembled into a 3D graphene-Au aerogel (GA/Au) via γ-ray irradiation technology. The XRD illustrated that the spectrum of GA/Au exhibited the characteristic diffraction peak of rGO (0 0 2) crystal plane at $2\theta = 23^{\circ}$ without the characteristic peak of GO (0 0 1) crystal plane at $2\theta = 10.8^{\circ}$, a strong indicator of GO reduction. The Bragg reflections at $2\theta = 38.3$, 44.6, 64.5, 77.4, and 82.4° corresponded to single crystalline AuNPs, verifying the reduction of Au^{3+} to AuNPs. The SEM showed that the composites had a 3D porous network that originated from the self-assembling of rGO due to the restoration of rGO's π–π conjugated structure [92].

Graphene-Copper. Successful reduction of GO in the presence of copper (Cu) to obtain rGO-Cu composites with enhanced electrical conductivity and inhibited aggregation of Cu NPs was reported by Nurfiana et al. [93]. The rGO-Cu composite was obtained after γ-radiolysis of the precursors under alcoholic conditions at an optimal dose of 35 kGy. The cyclic voltammetry indicated an increase in the electroactive trough of the as-prepared composite. During the charge and discharge process, rGO maintained a conductive network for electron transfer, and CuNPs in rGO enhanced access to electronic and ionic transport channels.

Graphene-metal oxides composites

In semiconductors such as ZnO [94] and SnO_2 [95], the penetration of γ-radiation causes structural defects such as oxygen vacancies, that vary with the total doses. Optimal doses also increase the crystallinity of metal oxide thin films while reducing the particle size [94]. This literature agrees with [96] findings who observed that applying 125 kGy yielded polycrystalline NPs with a crystallite size of 49.27 nm versus 261 nm at 0 kGy. The dislocation density, macrostrain and the band gap also decreased from 3.8 eV to 3.4 eV with the increase in doses thereby improving the conductivity. Similar observations were made by [97] on Fe_2O_3 films.

Graphene sheets undergo significant agglomeration and re-stacking during reduction and drying due to the Van der Waals interactions between its layers, consequently compromising its performance in the various fields. The development of graphene/metal oxide composites promises to be a successful approach for harnessing all the prospective advantages of graphene and metal oxides in respective applications [98]. Like in graphene/metal hybrids, graphene's responsibility in a graphene/metal oxide composite is to support metal oxides, induce the nucleation, growth, and formation of fine metal oxide nano/microstructures with uniform dispersion and controlled morphology on the

surface of graphene with high chemical functionality [99]. In addition to suppressing graphene's agglomeration and re-stacking, the metal oxide component offers excellent conductivity, capacitence, and other properties based on its size, shape, and crystallinity. The enhanced properties are consequent to the formation of a perfectly integrated structure with a developed electron conductive network and shortened ion transport pathways. Metal oxides also increase the accessible surface area of graphene thus promoting its electrochemical and catalytic activities to mention a few. These synergistic effects in graphene/metal oxide hybrids occur due to size effects and interfacial interactions via reactive chemisorption on the oxygen carrying moieties of graphene that bridge metal centres at oxygen-defect sites and Van der Waals interactions between the pristine region of graphene and metal oxides [100].

The fabrication of graphene/metal oxides composites has been explored efficiently in other radiation techniques such as microwave radiation [101]. Although the exploration of graphene-metal oxide composites for various applications using the γ-ray irradiation is at its infancy stage, there are several reports on the fabrication of graphene-metal oxide composites via γ-ray irradiation for catalytic applications where graphene (GO/rGO) serves as an electron collector and pathway to enhance the catalytic efficiency of the composites.

Graphene-Titanium oxide. Using γ-radiolytic method, TiO_2-rGO composite was synthesized in a solution of water and ethanol by doping TiO_2 with different amount of GO. The schematic of TiO_2-rGO composite synthesis in Fig. 5a-i depicts that the reduction of GO to rGO by γ-radiolysis occurs before the attachment of TiO_2NPs on the rGO layers. The TEM in Fig. 5a-ii displays the incorporation of homogeneously dispersed TiO_2NPs. The size of the TiO_2 NPs ranged between 20–25 nm. The decline and disappearance of intensity of the 2D band in the Raman spectra in Fig. 5a-iii signifies an increase in charge concentration due to doping with rGO [102]. The reduction of GO to rGO was confirmed by the I_D/I_G ratio that was enhanced after γ-ray induced reduction process and the optimum was reached at 1 wt% rGO, which supports the availability of high charge concentration on rGO and its interaction with TiO_2. The Raman peaks position of TiO_2 at 144, 397, 523 and 649 cm^{-1} remain at the same position, which confirms absence of structural change in TiO_2 even in the composite [103]. In another study TiO_2 nanotubes/rGO (rGO − TNTAs) were synthesized by γ-radiolysis at 20 kGy. The observations corroborated the previous study in that the γ-irradiation induced partial reduction of GO and the rGO − TNTAs was smooth with loosely lamellar structure. Additionally, the Raman suggested a reduction of GO through the diminishing of the 2D peak intensity [104].

Graphene-Zinc oxide. Azmy and colleagues fabricated zinc oxide-graphene (ZnO−rGO) composites by preparing mixtures with varying quantities of GO that were gradually added to ZnO followed by sonication. To generate five-layered films, the obtained solution was spin-coated on a glass substrate using a photoresist spinner. The film samples were then annealed at 350 °C to eradicate the excess precursors, reduce the GO, and provide a homogeneous coating for the ZnO-rGO. The thin films were later irradiated by ^{60}Co γ-source at 10 kGy at room temperature (Fig. 5b-i). The intensity of the (0 0 2) facet in the XRD spectra as well as other facets was enhanced for the radiated sample compared to un-radiated films (Fig. 5b-ii and iii) [105] due to pore formation that was effected by the γ-irradiation process [106]. The un-radiated samples (Fig. 5b-iv) have rougher surface (roughness value 14.9 nm), whereas the surfaces of the radiated samples were smoother because of smaller crystallite sizes with a roughness value of 4.67 nm (Fig. 5b-v).

Graphene-Iron oxide. Fe_2O_3/rGO nanocomposites with varying wt.% Fe_3O_4 was reported by Liang and Lu who prepared different concentrations of aqueous GO solution and added them into iron (III) hydroxide solution, followed by IPA. After purging under N_2, the suspensions were irradiated at ~ 170 Gy/min. The metal precursor and GO were reduced to Fe_3O_4 and rGO respectively. The formation of the nanocomposites was confirmed by the FTIR spectra as shown in Fig. 5c-i. For the nascent Fe_3O_4 and Fe_3O_4/rGO composites, transmittance signals for C=O and epoxy were weakened, while the characteristic absorption peak at 577 cm^{-1} attributable to the Fe–O bond emerged. The phase composition was confirmed by the Raman spectroscopy as shown in Fig. 5c-ii. Two peaks at 1340 cm^{-1} and 1600 cm^{-1} attributed to D and G bands of graphene are apparent in the spectra of GO and Fe_3O_4/rGO. The broad signal at 680 cm^{-1} was due to A_{1g} mode of Fe_3O_4 phase [107]. In addition, the peaks at 218 cm^{-1}, 286 cm^{-1}, 398 cm^{-1}, 592 cm^{-1}, and 1303 cm^{-1} originated from the decomposition of Fe_3O_4 to Fe_2O_3 by the high energy 532 nm laser light used in Raman spectroscopic analysis [108]. The results were comparable to that obtained by Kumar et al. [109] where dry microwave irradiation of Fe_3O_4/rGO was carried out and the hybrid material exhibited rGO nanosheets that were homogeneously covered by nearly uniform-sized Fe_3O_4 nanoparticles.

Graphene-polymer composites prepared via γ-radiolysis

When subjected to γ-rays, polymers undergo chemical and structural changes, resulting to the generation of free radicals, atom displacement, and carbonization. This process induces beneficial polymerization, crosslinking, and grafting of various polymer hybrids [110]. The radiation also reinforces the interfacial connections between organic polymers and inorganic NPs and enhance properties that are dependent on the microstructure and crystallinity such as optical and electrical properties [111]. The addition of rGO to polymers further enhances electrical conductivity and percolation threshold [112], improves the modulus and tensile stress [113], and enhance mechanical properties for polymers. These polymeric-graphene hybrids therefore can be applied in various electrochemical fields such as batteries, supercapacitors, and sensors [110]. γ induced polymer grafting, and crosslinking during the synthesis of graphene-polymeric nanocomposites is therefore worth exploring [114]. The following section presents recent works on γ-radiolysis of graphene-polymer composites.

To increase the efficacy of polyacrylamide-acrylic acid (p(AM-AA) in removal of strontium and cobalt ions from aqueous solutions, a p(AM-AA)-GO composite was synthesized via the template polymerization technique using γ-radiation as an initiator (40 kGy) as presented in Fig. 6a. Fig. 6b shows a porous and irregularly shaped p(AM-AA) while p (AM-AA)-GO has channels instead of pores (Fig. 6c), both the features encourage adsorption. As seen in Fig. 6d and e, the addition of GO to p (AM-AA) increased the adsorption efficacy for cobalt ions from 210 mg/g to 296 mg/g and strontium ions from 192 mg/g to 260 mg/g [115]. When composite films of poly (methyl methacrylate)-reduced graphene oxide (PMMA)-rGO (PrGO) were synthesized using solvent evaporation and subjected to varying doses of γ-ray radiation (25–100 kGy), semi-crystalline PMMA (Fig. 6f) were obtained according to the XRD. While the intensity changes were insignificant at 15° and 25° for PMMA and rGO respectively, the PMMA signal at 30° vanished upon radiation due to polymer scission. The SEM micrographs of ProGO films in Fig. 6g exhibits a smooth surface but after irradiation with 50 kGy (Fig. 6h) lamellar structures were evident on the surface due to thermal fluctuations. Elevated dosage (100 kGy) resulted in the formation of pores, a phenomenon ascribable to double network between rGO and the polymer as shown in Fig. 6i. According to the AFM, the surface of the composite was 3.5-fold rougher than the nascent polymer after irradiation at 50 kGy dose while after 100 kGy the surface was 2-fold smoother than the pristine composite as shown in Fig. 6j. [116]. Another study reported that γ-irradiation induces chain scissions in the bonds associated with the C=O stretching in polypyrrole/GO composites. The XRD peak intensity declined with the increase in the GO concentration in PPy after γ-irradiations, whereas the reverse trend was observed before the irradiation of the samples [117].

The durability and resilience to wear for polyvinyl alcohol/graphene

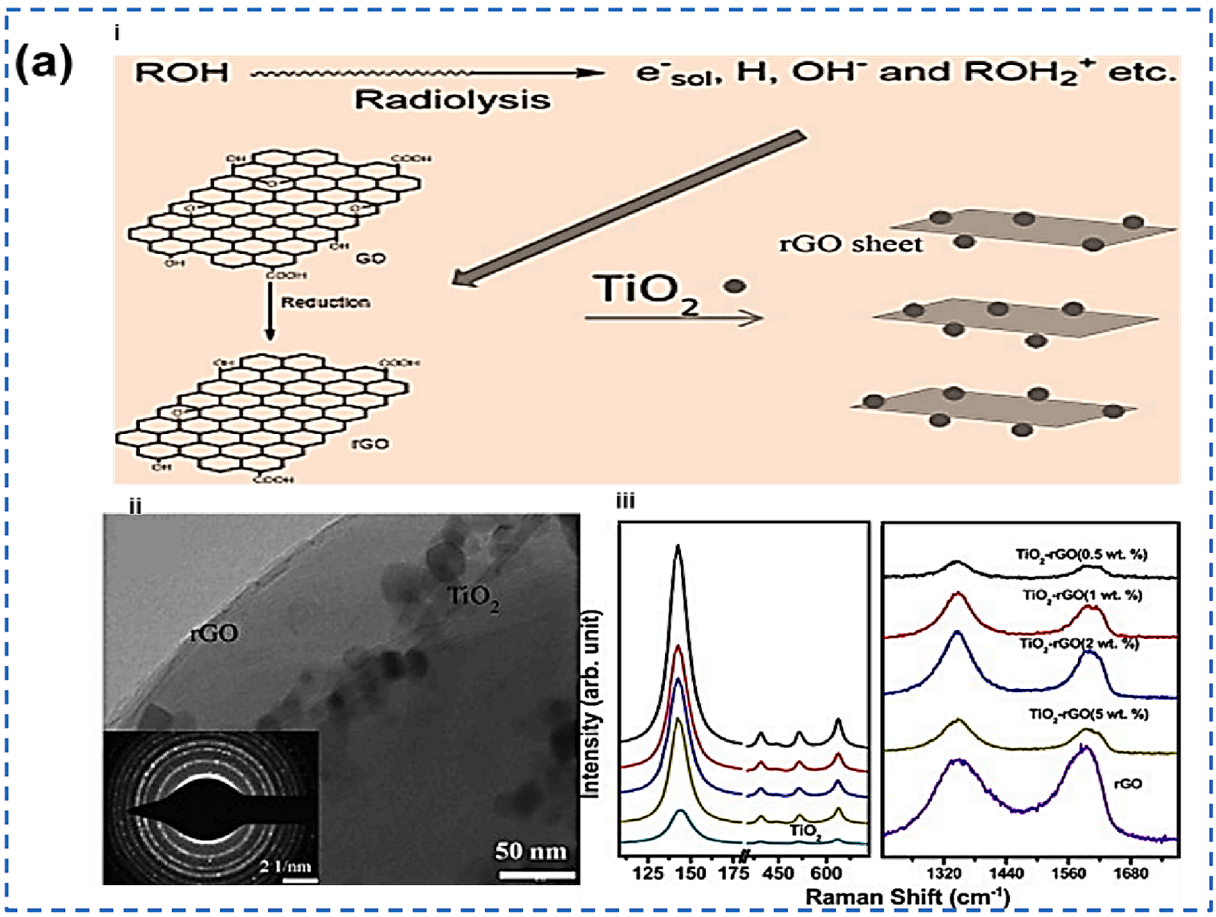
(a)
i
ROH
Radiolysis
e⁻sol, H, OH⁻ and ROH2⁺ etc.
GO
Reduction
rGO
TiO2
rGO sheet
ii
rGO
TiO2
2 1/nm
50 nm
iii
Intensity (arb. unit)
TiO2
TiO2-rGO(0.5 wt. %)
TiO2-rGO(1 wt. %)
TiO2-rGO(2 wt. %)
TiO2-rGO(5 wt. %)
rGO
125 150 175 450 600
1320 1440 1560 1680
Raman Shift (cm-1)

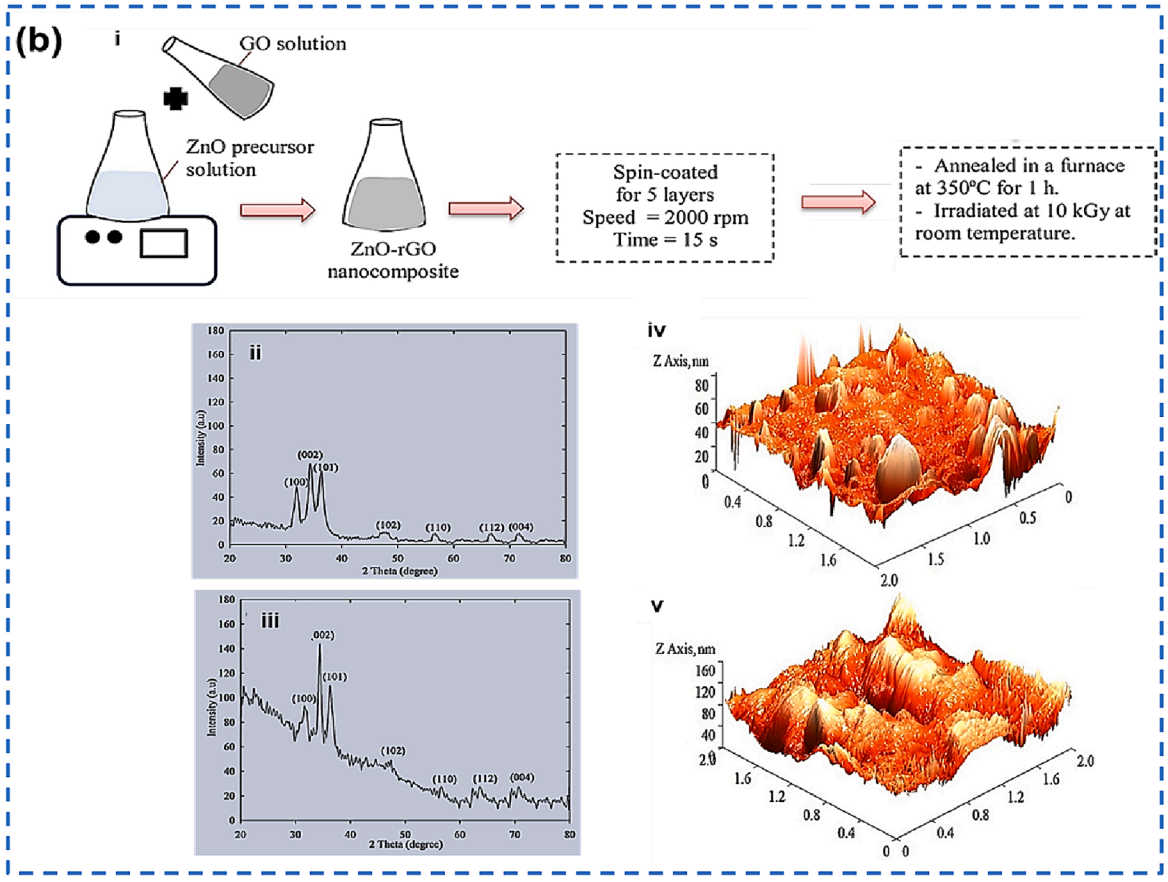
(b)
i
GO solution
ZnO precursor solution
ZnO-rGO nanocomposite
Spin-coated for 5 layers
Speed = 2000 rpm
Time = 15 s
- Annealed in a furnace at 350°C for 1 h.
- Irradiated at 10 kGy at room temperature.
ii
Intensity (a.u)
(002)
(101)
(100)
(102)
(110)
(112)
(004)
2 Theta (degree)
iii
Intensity (a.u)
(002)
(101)
(100)
(102)
(110)
(112)
(004)
2 Theta (degree)
iv
Z Axis, nm
v
Z Axis, nm

Fig. 5. (a-i) Schematic representation of TiO_2-rGO composite formation by γ-radiolytic process, (a-ii) TEM image of TiO_2-rGO composite. Electron diffraction pattern of TiO_2-rGO composite (Inset), (a-iii) Raman spectra of TiO_2-rGO nanocomposite for different wt. %. Zoomed part revealing rGO Raman feature (Inset). Reproduced with permission from ref. [103]. Schematic illustration (b-i) synthesis of ZnO-rGO nanocomposite thin films by gamma radiation via sol–gel method, XRD images of un-radiated (b-ii) and radiated (b-iii) ZnO-rGO nanocomposite, AFM micrographs of un-radiated(b-iv), and radiated (b-v) ZnO-rGO nanocomposite thin films. Reprinted with permission from ref. [105]. (c-i) FTIR spectra and (c-ii) Raman spectra of GO sheets, of GO sheets, bare Fe_3O_4, Fe_3O_4/rGO-1, Fe_3O_4/rGO-2, Fe_3O_4/rGO-3, and Fe_3O_4/rGO-4 composites. Reprinted with permission from ref. [108].

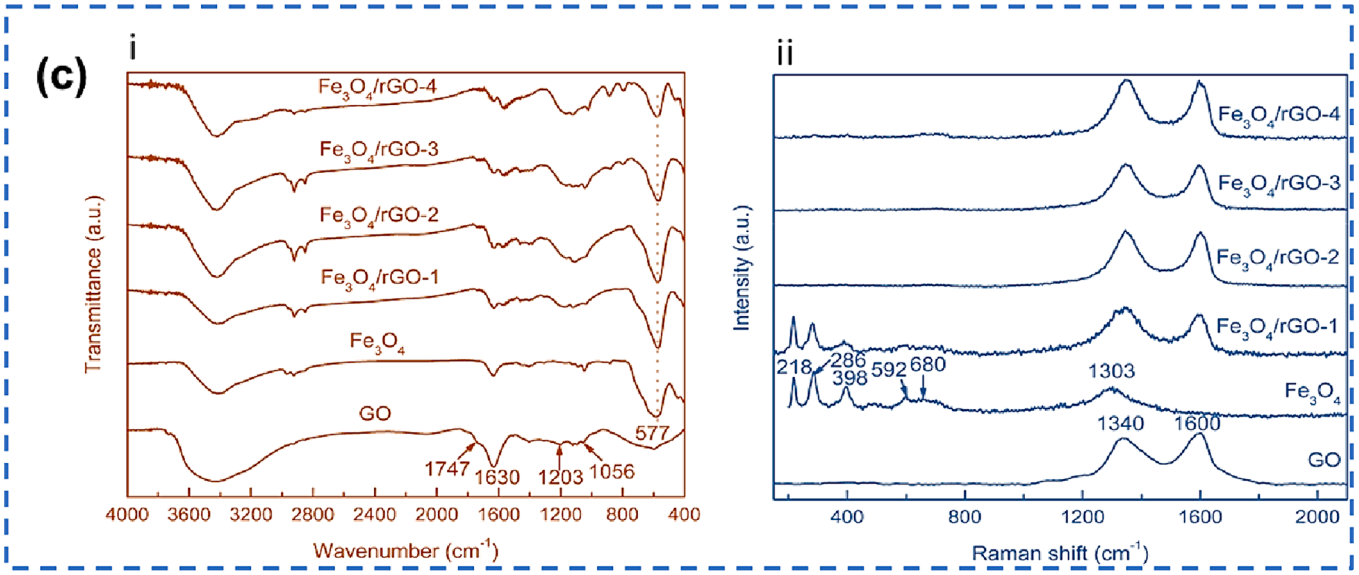

Fig. 5. (*continued*).

oxide (PVA/GO) hydrogels was enhanced via irradiation. The PVA/GO hydrogels were prepared using the freeze–thaw method followed by an in-*situ* reduction by subjecting the hydrogel matrix to doses of 50, 100, 150, and 200 kGy of γ-ray irradiation. The rGO served as the cross-linking site for the dangling bonds between molecular chains and formed covalent bonds. The irradiated PVA/GO showed 270 % improvement of compressive strength at 150 kGy compared to unirradiated hydrogels [118]. Using γ-ray radiation as the initiator, aniline was graft copolymerized onto graphene and cellulose to form double network hydrogels in one-pot. The resulting graphene-polyaniline-cellulose graft copolymer's crosslink density increased from 0.0297 at 40 kGy to 0.0908 at 80 kGy. The conductivity elevated form 2.012 x 10^{-2} Scm^{-1} to 4.766 x 10^{-2} Scm^{-1} which boosted the capacitance of the hydrogel as well. Higher doses caused a slight decline of the specific capacitance due to the breakage of the hydrogels crosslinks and the decrease of grafting yield [119].

Graphene-carbon nanotube hybrids

Due to outstanding electrical characteristics, strong mechanical stability, and thermal stability, large surface area 1D carbon nanotubes (CNTs), like graphene have garnered a lot of attention. These salient properties qualifies CNTs in a lot of applications such as energy storage [120], photocatalysis [121], adsorption [122], sensing [123] etc. Therefore, fabricating graphene/CNT hybrids to obtain synergistic effect of the two materials is plausible. Introducing 1D CNTs to 2D graphene not only lowers the aggregation of graphene, it also results into the formation of interwoven 3D conductive channels that strengthen the mechanical properties of the CNT/Graphene composite [124]. Although GO/CNT hybrids have been prepared via different techniques, the synthesis methods are complex and expensive [125]. In addition, the uneven contact and irregularities between CNTs in the heterogeneous structure limit their application [126]. As such better synthesis techniques to address the mentioned challenges are a necessity. In this regard, the γ-irradiation synthesis method for the GO/CNT composites has been reported.

To that effect, 3D graphene functionalized multiwalled carbon nanotube (Gr-f-MWCNT) hybrids has been reported by [127] who hybridized GO with acid functionalized (f-MWCNTs) via γ-radiolysis in an alcohol-water medium. When compared to GO and MWCNTs separately, the hybrid showed less self-aggregation and stacking, which improved Gr-f-MWCNT's stability, electrocatalytic activity, and conductivity. The effect of γ-irradiation on the formation of the composite was confirmed by UV–Vis where the GO spectra showed a 230 nm peak due to the transitions of C-C aromatic ring and shoulder at 308 nm corresponding to transition of C=O bond, the f-MWCNTs absorption peak was positioned ~ 260 nm prior to irradiation. After irradiation, the Gr-f-MWCNTs hybrid consisted of four peaks at 208, 225, 275, and 281 nm. The 275 nm red-shifted from 230 nm of GO while the 281 nm red-shifted from 260 nm inf-MWCNTs. The significant red shift of peaks in the hybrid was due to an increase in electron density and structural ordering consistent with the restoration of sp^2 carbon atoms. The red shift also confirmed the π-π stacking interactions between the aromatic basal planes of GO and MWCNTs. The new peaks at 208 and 225 nm were ascribed to the formation of C-H bonds simultaneous to C-C bond breaking [128]. Another 3D hierarchical composite of rGO/acid-treated multi-walled carbon nanotubes (rGO/aMWCNT) was fabricated by dispersing GO in IPA-water solution containing aMWCNT before being exposed to irradiation (Fig. 7a). Fig. 7b-i present the HRTEM image of transparent and crumpled rGO nanosheets sheets. The rGO/aMWCNT has aMWCNT (red arrows) that are uniformly distributed between the layers of rGO nanosheets, resulting in the formation of 3D interpenetrating network structure (Fig. 7b-ii). The C/O weight ratio in rGO/aMWCNT increased with the irradiation dose, reaching the maximum of 6.9 at 100 kGy, and slightly decreased at higher doses (Fig. 7c). Meanwhile, the trend of the conductivity followed the C/O weight ratio of rGO/aMWCNT (Fig. 7d) an affirmation that the irradiation dose has significant influence on the reduction of RGO/aMWCNT. Additionally, the optimised rGO/aMWCNT (GO: aMWCNT ratio = 80:20) presented a large specific surface area (1420 $m^2\ g^{-1}$) compared to 700 $m^2\ g^{-1}$ of pristine graphene [124]. Ma and colleagues prepared a suitable aqueous mixture of GO/CNTs, and irradiated the sealed solution at 300 kGy with radiation rate of 200 Gy/min. An aqueous solution of the obtained GO/

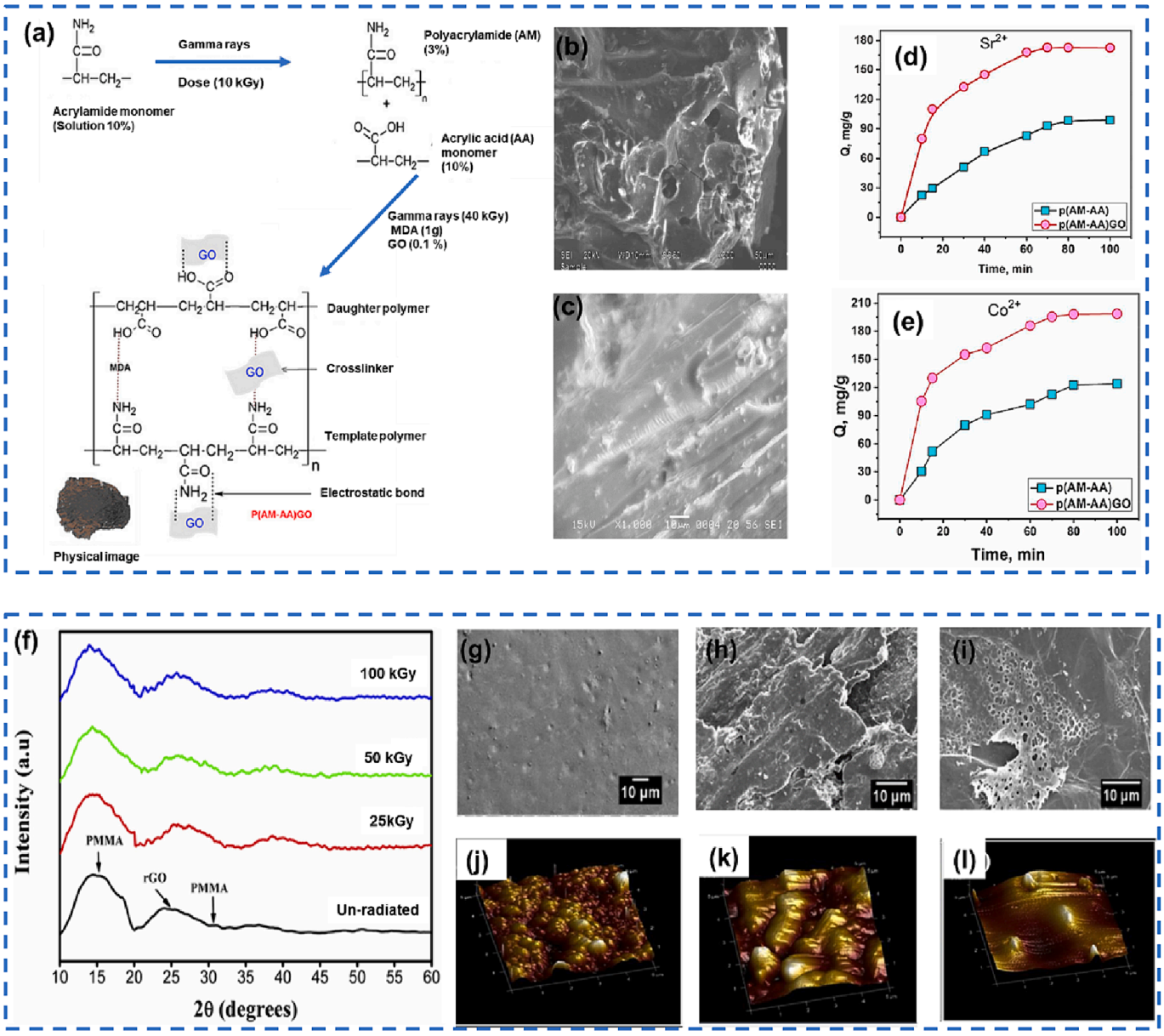

Fig. 6. (a) Schematic preparation of p(AM-AA)GO by γ radiation at 40 kGy from the acrylamide monomer and acrylic acid monomer containing GO, SEM images for (b) porous p(AM-AA) and (c) channelled p(AM-AA)GO, absorption efficiency of p(AM-AA) and p(AM-AA)GO on (d) Sr^{2+} and (e) Co^{2+}. Reprinted with permission from ref. [115], (f) XRD spectra for PrGO the thin films at various irradiation doses, SEM images of the thin films (g) PrGO, (h) PrGO-50 and (i) PrGO-100,3D, AFM images of the films (j) PrGO, (k) PrGO-50, and (l) PrGO-100. Reprinted with permission from ref. [116].

CNT composite was added into a PVA solution to get PVA/GO/CNTs composite films. The resulting PVA composite films outperformed the nascent PVA in terms of mechanical properties, achieving a tensile strength of 81.9 MPa and a Young's modulus of 3.9 GPa, respectively. These substantial advancements were credited to the robust hydrogen bonding between GO/CNTs and PVA chains, uniform dispersion, and the interlinked 3D structure of GO/CNTs [129].

Graphene-Ionic liquids composites. Ionic liquids (ILs) are organic salts that are in the liquid phase at room temperature. Since most ILs are produced using less harmful methods than traditional solvents, they are regarded as "green" solvent alternatives to volatile organic compounds. Compared to other functionalizing molecules, ILs provide the greatest flexibility because of the inexhaustible possibility of theoretical cation–anion interactions, high thermal/chemical stabilities, and low vapor pressures [130], non-flammable, wide electrochemical stability, and high ionic conductivity [131]. ILs also exhibit favourable characteristics such as hydrophobic attraction, H–bonding, π–π interactions, dipole–dipole interaction, and electrostatic interaction with other molecules [132]. These molecules reportedly alleviate agglomeration and stabilises each graphene sheet via electrostatic and cation-π interactions [133]. Graphene modified by ILs not only has stable structure but also has a high charge transfer rate, which improves its electrochemical performance [131]. Numerous hybrids of graphene/ILs and graphene/metal oxide-ILs have been constructed for different applications including electrode model construction [134], gas separation [135], supercapacitors [131], sensors [136], and adsorption [137] to name a few.

In as much as graphene-ILs hybrids have been intensively studied only a handful of them has been synthesized via the γ-irradiation technique. Owing to the ability of ILs to stabilize metal NPs by capping them [138], Ag and GO were simultaneously reduced at room temperature via

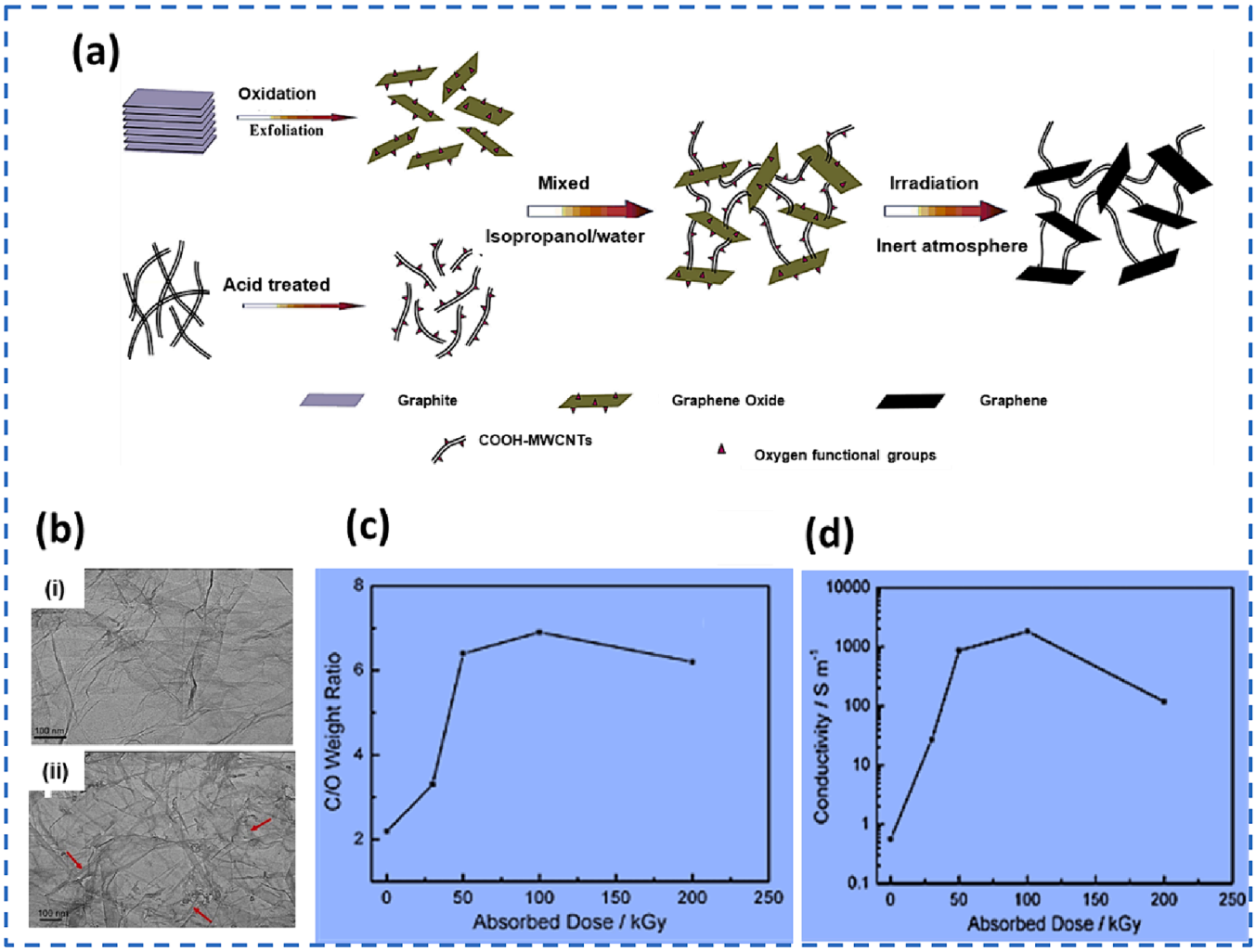

Fig. 7. (a) Schematic illustration for preparing hierarchical rGO/aMWCNT composite by irradiating a mixture of water-isopropanol medium, GO and acid treated MWCNT in inert atmosphere at room temperature. (b) TEM micrographs for crumbled rGO sheets (i), 3D interpenetrating network of rGO/aMWCNT (ii), (c) Plot of C/O weight ratio versus the irradiation dose, (d) Plot of conductivity versus the irradiation dose for rGO/aMWCNT. Reprinted with permission from ref. [124].

γ-irradiation at 160 kGy with the assistance of IL (EMImAc) to obtain Ag-rGO-IL hybrids. The TEM images revealed that although AgNPs on the surface of Ag-rGO were uniformly distributed, the size distribution and dispersibility of AgNPs was perfectly homogeneous in Ag-rGO-IL samples. This was because the IL wrapped itself around the AgNPs thereby regulating their size and prevented their agglomeration on the surface of the formed rGO. At the same time, it reduced the formation of wrinkles on rGO. The C/O ratios were 2.8 and 8.7 for Ag-rGO and Ag-rGO-IL, respectively signifying the importance of EMImAc in the reduction of GO. The TGA curves revealed ~ 25 % weight loss at 200 °C in Ag-rGO compared to only 5 % loss in Ag-rGO-IL [139]. In a novel study, radical polymerisation for the synthesis of GO and IL (GO@IL) using 3-n-Hexadecyl-1-vinylimidazolium bromide ($[C_{16}VIm^{\pm}]$ $[Br^{-}]$) as the monomer via γ-ray irradiation at 15 kGy in one step was carried out as illustrated in Fig. 8a. The XPS spectra shown in Fig. 8b indicated that the main elements in the GO spectra are C and O, while the GO@IL consist of the N and Br peaks with elevated intensities. These elements originated from $[C16VIm^{\pm}]$ $[Br^{-}]$ as such the XPS confirmed the functionalization of GO by the IL. The TEM image presented in Fig. 8c where GO has wrinkles at the edges (c-i), due to Van der Waals interaction however after undergoing radical polymerization with $[C_{16}VIm^{\pm}]$ $[Br^{-}]$, multiple black spots were formed within the layers of GO without observable deformation from irradiation (c-ii), verifying grafting of IL monomer onto GO surfaces. The adsorption capacities of GO@IL for Sunset Yellow (SY) and chromium VI (Cr VI) in acidic media at room temperature were 169.6 and 75.8 mg g^{-1} respectively as presented in Fig. 8d and e. These pollutants were adsorbed to the composites via electrostatic and π − π stacking interactions of the composite [140].

Factors affecting GBMs during γ-ray irradiation

It has been suggested in earlier findings that modulating the synthesis conditions, such as irradiation dose and irradiation rate, pH, and the source of radicals influence the morphology and hence the possible applications of γ-synthesised materials [38]. Therefore, there exist a need to find the optimal point of every reaction parameter during the preparation of nanomaterials, even GBNMs.

Total irradiation dose

The irradiation dose has been reported to influence the structure of GBNMs. In that regard, Dumée's group reported an increase in the density of the crystalline graphitic walls of graphene at higher dose (100–300 kGy) based on the TEM results [47]. In the case of graphene aerogels, it was observed that low doses produce partially reduced GO sheets with a tendency to restack together however the self-assembly process into 3D structure was incomplete [46]. The self-assembly was enabled by the ability of γ-rays to strip, reduce and crosslink graphene.

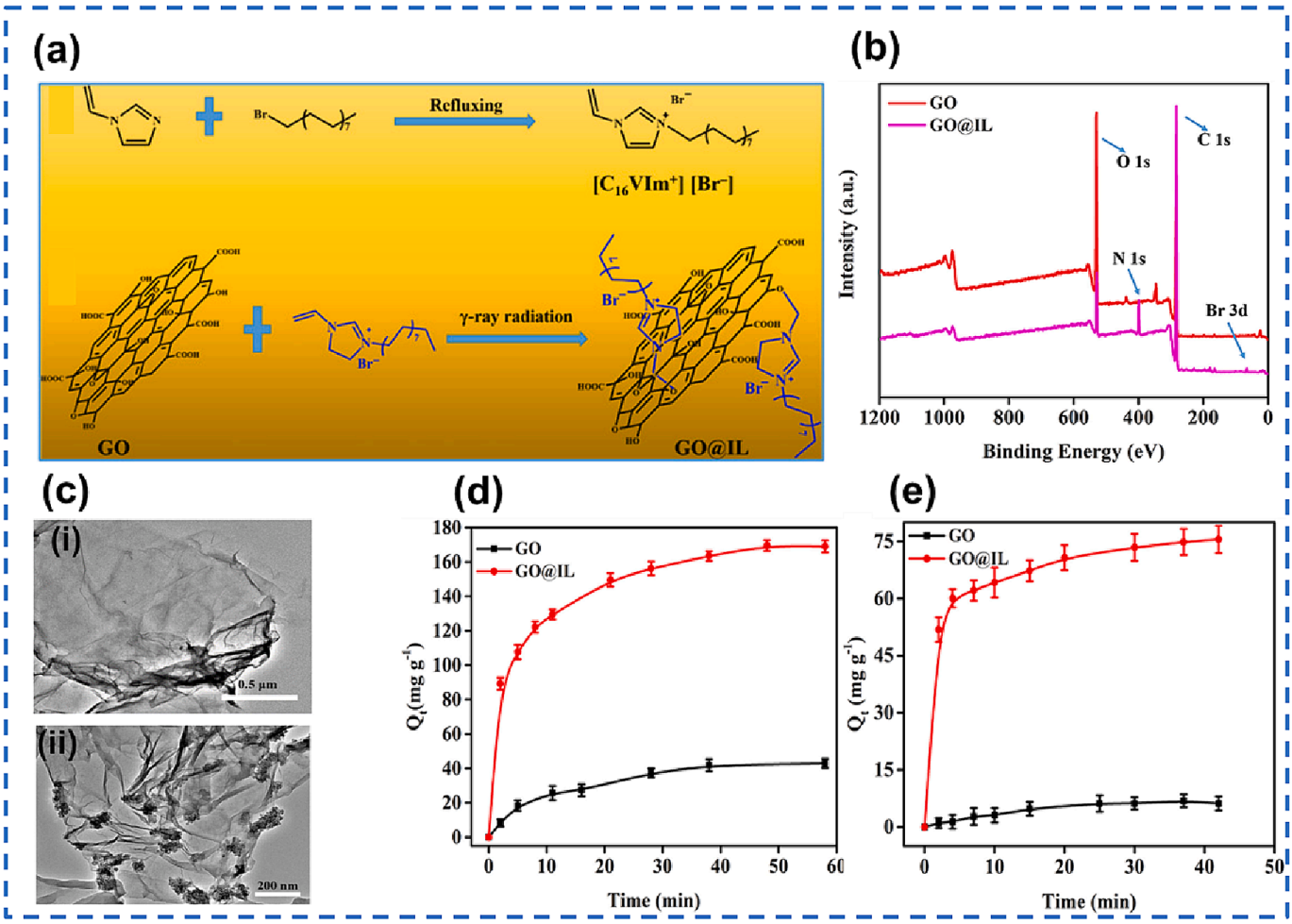

Fig. 8. (a) Diagrammatic representation for the fabrication of GO@IL from a separately formed [$C_{16}VIm^{\pm}$] [Br^{-}] and GO solution one-step γ-irradiation functionalization, (b)XPS spectra of GO and GO@IL, (c) TEM micrographs of for GO (i) and GO@IL (ii), The impact of contact duration on adsorption of (d) SY or (e) Cr (VI) by GO and GO@IL (10 mg Adsorbent,; with 50 mgL^{-1} SY concentration, 30 mg L^{-1} Cr(VI) concentration, at pH = 7 for SY, pH = 2 for Cr (VI); temperature, 298 K). Reprinted with permission from ref. [140].

PVA-GO hydrogels where GO served as crosslinkers were prepared by the freeze–thaw technique as shown in Fig. 9a. The formed radicals and electrons that were solvated with PVA reduced the GO in the PVA matrix (Fig. 9a). The SEM image in Fig. 9b-1 for unirradiated PVA-GO hydrogel showed a homogenous 3D porous network but after exposing the composite to γ-irradiation, a denser and more compact structure was apparent. Also, the pore size was reduced with increasing irradiation dose from 50-200 kGy as shown in Fig. 9b-2 and b-3, a phenomenon that was ascribed to perfect crosslinking induced by γ-irradiation. Fig. 9c shows the XRD patterns of GO, plain PVA, and PVA/GO hydrogels treated with various radiation dosages. Subjecting the hydrogel to higher doses resulted to a slight shift in the position of the diffraction and the intensity of the peak dropped dramatically in comparison to that of the non-irradiated sample. This implies that elevated irradiation doses significantly decrease the crystallinity of the formed hydrogel.

Since altering the morphology and crystallinity of nanomaterials has a direct influence on their performances in various applications, it is not surprising that graphene composites prepared at different doses display differences even in their performances. In that note, γ-radiated PVA/GO hydrogel composites exhibited enhanced compressive mechanical property(270 %) due to crosslinking at optimal dose. The increase in total dose also improved the electrical conductivity of rGO. As such the conductivity of rGO prepared at 80 kGy (0.170 $S{\cdot}m^{-1}$) was higher than that prepared at 40 kGy (0.160 $S{\cdot}m^{-1}$) owing to differing reduction degrees [55]. To investigate the effect of irradiation on supercapacitor electrodes, $ZnCo_2O_4$-rGO samples were exposed to gamma rays at doses of 5, 10, 15, 25, and 50 kGy. The sample that was exposed to the highest amount of γ-radiation showed the highest specific capacitance (365 Fg^{-1}), maximum stability after 5000 cycles and the lowest charge transfer resistance. The low charge resistance proves that the improved supercapacitance at the highest dosed electrode material was due to enhanced conductivity since the capacity of supercapacitors depends on the conductivity of the electrodes [141]. In polymeric nanocomposites the total adsorbed does is usually small because polymers undergo chain scission at higher doses which tempers with the stability and function of the composites [40]. The same observations were made by [142], who constructed a photocatalytic AgNPs/rGO-*TNTAs composite for degrading ethylene by mixing the precursors in water and 1 wt%. PVP before exposing the mixture to irradiation at 10, 20 and 30 kGy. The optimal rate constant was obtained at 20 kGy after which it declined. The decline was attributed to larger size of AgNPs at the 30 kGy that formed due to γ-rays inducing chains scissions in the polymer matrix (PVP) therefore releasing of AgNPs allowing them to aggregate thereby reducing the photocatalytic surface area. Alternatively at 30 kGy dose the solvation shell of the growing colloids was probably destroyed which led to disruption of the charge equilibrium on the composite's surface.

Dose rate

Exposing graphite to 2 MGy radiation showed more flaws and a

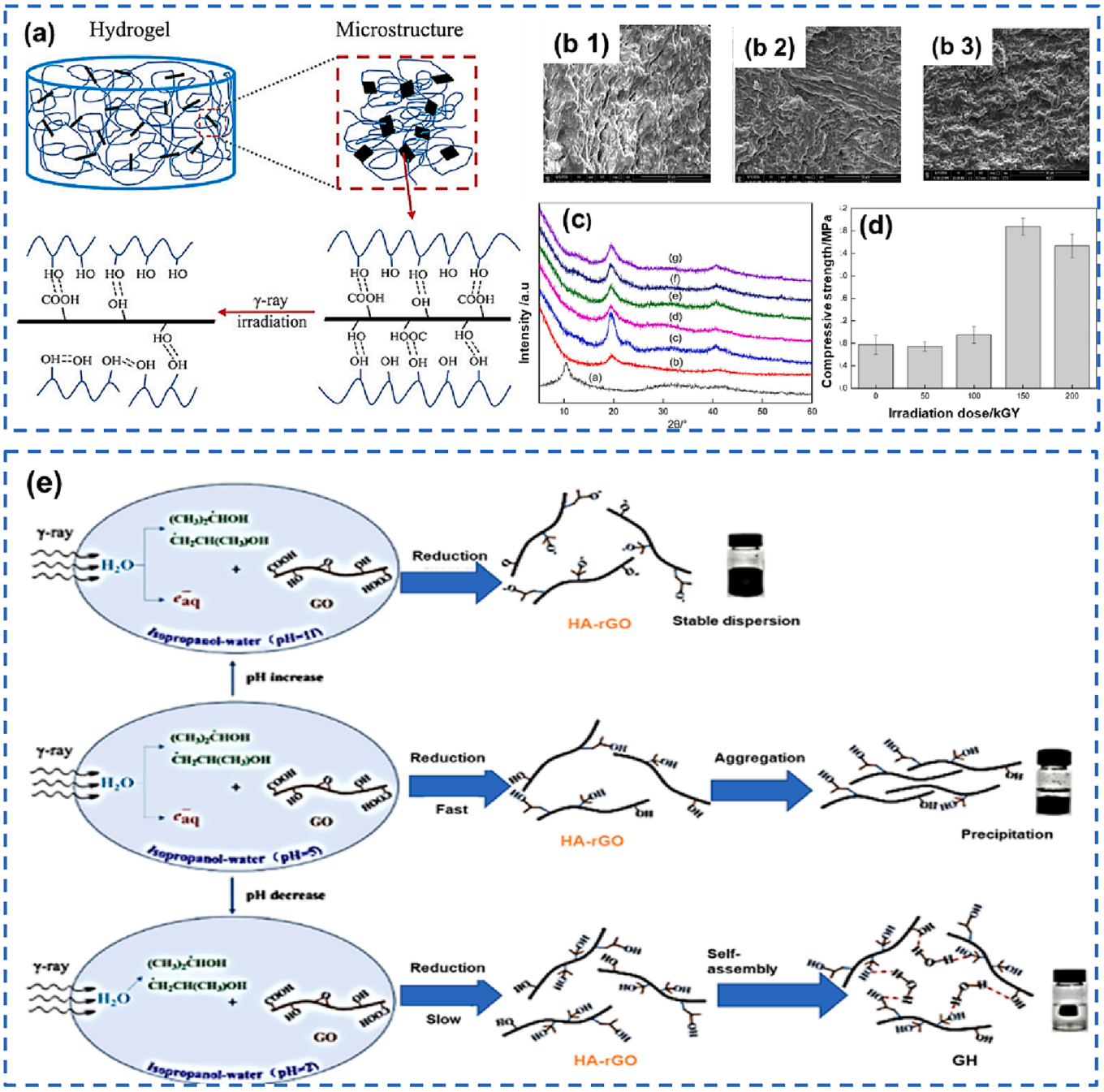

Fig. 9. (a) Synthesis of PVA-GO hydrogel formed by freeze drying PVA and GO where GO served as a crosslinker before irradiation at various doses, (b1-3) SEM micrographs showing reduction of pore size with as the dose was elevated, (c) XRD spectra (d) showing the impact of radiation exposure on PVA-rGO hydrogels' water content. Reprinted with permission from ref. [118]. (e) The generation of HA-rGO by γ-radiation and its aggregation patterns in an isopropanol-water media at varying pH values. Reprinted with permission from ref. [47].

lower extent of graphitization than graphite exposed to 200 kGy radiation [143]. Surprisingly, these results were inconsistent with Galvan et al. [144] who found that γ-irradiation increased the amount of turbostratic graphite with a total dose of 1 MGy at a rate of 8.4 kGy/h in graphite. The inconsistency of the result was ascribed to the difference in the irradiation rate between Li's group and Galvin's group which was 1.8 kGy/h, and 8.4 kGy/h respectively. An elevated irradiation dose rate generates higher density quantas that produces more recoiled electrons with high energy via Compton scattering which destroys the graphene plane rather than anneal it via sputtering mechanism [143]. The dose rate also affects γ-radiosynthesis of metallic nanoparticles, which is crucial when GO is used as a support material. For example, high dose rates were reported to yield smaller MNCs with a narrow size distribution because the reducing agents are produced rapidly and scavenged within the medium while at low dose rates bigger MNCs are formed with a larger size distribution because interactions between the metal ions and other atoms and coalescence processes are faster than the generation rates of reducing species [145].

pH

The pH of the medium to be irradiated affects the precipitation of the formed GBNMs and thus has a strong influence. As such, the medium's pH should be carefully controlled to improve the efficacy of

γ-radiosynthesis of graphene-based aerogels. In this regard, Wang et al. observed that at low pH (pH 2) of t-butanol-water medium, the principal active species convert into alcoholic radicals ($^{\bullet}CH_2(CH_3)_2COH$) with high reducing capacity to react with the reactive groups of GO nanosheets. The generated reducing agents simultaneously reduce and hydroxyalkylate GO sheets under γ-ray radiation. Further, the OH groups form hydrogen bonds with water molecules. This occurs concurrently with the strong π-π conjugation between rGO, which triggers the radiation-modified nanosheets' self-assembly and results in the formation of a free-standing monolithic graphene hydrogel. However, under strong basic conditions (pH 11), the hydroxyalkylation degree of GO nanosheets is lower due to a low quantity of primary radiolysis active free radicals which can be transformed into $^{\bullet}CH_2(CH_3)_2COH$ compared to the strong acidic condition [23]. The same group conducted a similar study where t-butanol was replaced by isopropanol to obtain 3D graphene aerogels. The observation was the same. The best aerogels were also obtained at lower (pH=2). These possessed the lowest density (4 mg/cm^3) while could support up to 18 g without crumbling. The density of the aerogel was lower than those of chemically synthesized aerogels [45].

Source of radical species

The source of radical species can be gaseous (H_2, N_2) [51] or the common liquid media (alcohols, formate ions, ethanediamine, etc) [28,46]. The difference in the radicals is that they exhibit different ionization energies, and relative molar concentrations in case of gaseous sources. For example, O_2 can form radicals ($O^{\bullet}$, $H^{\bullet}$, and ozone (O_3)). Because of this, the molar concentration of O_2 in air is lower than that of N_2, which may prevent the production of oxidizing radicals that may scavenge the surface of GO sheets [51]. Where alcohols are concerned, their reaction constant have a significant impact. For instance, the reaction constants of $(CH_3)_3COH$ with OH and H are 12-fold lower than those of other alcohols. Moreover, its stearic hindrance is larger than of other aliphatic alcohol radicals, as such, a higher total dose is required to trigger the self-assembly of the GO nanosheets, compared to other alcohols [45]. When a study of the influence of various alcohols (methanol, ethanol, isopropanol, and t-butanol) on the γ-ray irradiation reaction was carried out, 1:1 (v/v) ratio of water to ethanol was the most effective. This was attributed to ethanol's higher rate constants for scavenging hydroxyl radicals [127].

Applications of GBMs modified by γ-radiolysis

According to literature γ-synthesised GBNMs have diverse applications including catalysis, energy-related, sensor, biomedical applications etc. Therefore better understanding of γ-radiosynthesis has the potential to enable large-scale production in the near future [146]. The next section summarizes the applications and advantages of γ-ray prepared GBMs.

Photocatalytic water remediation

Environmental pollution especially that of water is on the rise owing to population boom that lead to an incresed number of industries (agricultural, pharmaceuticals, textiles, etc.) that discard waste of various kinds in the water bodies [147]. Therefore, the need to come up with cheap and safe water remediation techniques is on the rise including biological, chemical, and physical means. The decontamination of the environment i.e water, via photocatalysis that breaks down microbes, dyes, used hormones, pharmaceuticals etc is superior to physical, chemical, and biological decontamination methods because photocatalytic degradation is cost-effective and environmentally benign. It involves a rapid oxidation/reduction process, and it can eliminate pollutants through mineralization [148]. Briefly, when a photocatalyst is irradiated by photons with an energy that is above the photo-threshold, the electrons (e^-) are excited from the valence band (VB) to the conduction band (CB). This forms positively charged holes (h^+) for every excited e^-. The newly formed electron-hole (e^-/h^+) pairs migrate to the surface of the photocatalyst where the e^- reduces the adsorbed O_2 to generate superoxide anion ($O_2^{\bullet-}$). The h^+ reduces H_2O and OH^- to generate $H_2O^{\bullet}$ radicals, named reactive oxygen species (ROS) that are responsible for the degradation of pollutants [149].

Carbon materials such as CNTs, carbon nanofiber, and graphene are widely used as support materials for photocatalysts such as TiO_2 [150], CdS Qds [142] etc. The carbon materials i.e graphene enhance the photocatalytic activity of the photocatalyst in various ways that include, improving light absorption by photosensitization through their electron-rich surface, their high electrical conductivity serves as electron sink thus reduce the charge recombination in the photocatalysts thus availing the photo-generated electrons (e^-) and holes (h^+) for the photocatalytic processes [151].

γ-radiosynthesis has proven to be the best alternative technique for production of graphene-based catalysts in an environmentally friendly and cost-efficient manner. Hareesh et al. [152] synthesized AgNPs, rGO and Ag-rGO via the γ-technique. The TEM reveals that the AgNPs were uniformly dispersed on the surface of the rGO (Fig. 10a) with an average size of 10 nm. The group later investigated the photocatalytic activity of the as-synthesized nanomaterials in photodegradation of methylene blue (MB) under visible light. The degradation kinetics in Fig. 10b show that the photocatalytic efficiency of γ-prepared Ag-rGO is approximately 9 and 5-fold higher than to that of AgNPs and rGO respectively. During the excitation of Ag-rGO, charge carriers (e_{cb}^-, h_{vb}^+) are generated by the AgNPs and the e_{cb}^- was subsequently transferred to the rGO sheet whose $\pi - \pi^*$ conjugation structure acts as an electron acceptor which promotes charge separation. This encouraged the formation of oxidative reactive radicals that degraded the MB dye as per the reaction scheme shown in Fig. 10c. The catalyst displayed 99.71 % photodegradation of MB dye which was reduced to only 92.89 % after the 8th cycle therefore a good cyclic performance. The γ-radiation cross-linking technique was employed during the preparation of chitosan/cobalt ferrite/graphene oxide (CS/CF/GO) nanocomposites catalyst. First, the CF and GO were separately dispersed in water and sonicated for 1 h. Then specific amounts of CF were added to chitosan dissolved in acetic acid before adding definite amounts of GO into the mixture (CS/CF). The mixture in the glass tube was then ultrasonicated and irradiated at 10 and 20 kGy at a dose rate of 1.2 kGy/h. The CS/CF/GO nanocomposites exhibited a photo-Fenton catalytic nature for the degradation of Maxilon C.I. basic dye in aqueous medium. As such, 99 % dye was removed in the presence of 10 mM H_2O_2 in the reaction system, compared to 70 % dye removal in the absence of H_2O_2 at 120 min of sunlight irradiation [153]. In a different study, cadmium sulfide quantum dots/ reduced graphene oxide (CdSQDs/rGO) nanocomposites were realized via a one-step γ-ray radiation induced reduction method. The optimal dose and feed ratio were 300 kGy and 1.0 wt% GO to $CdCl_2$ 2·.$5H_2O$ respectively. The composite degraded 93 % Rhodamine B in 250 min under visible light [154]. This technique was also employed to simultaneously transform TiO_2 nanotube arrays (TNAs) from an amorphous state to an anatase crystal state (*TNAs), synthesize CdSQDs and reduce GO to ultimately form a CdSQDs/rGO-*TNAs composite. The composite exhibited photocatalytic activity towards ethylene in a simulated cold-storage environment. The rate constant for ethylene degradation was $1.0^7 \times 10^{-3}$ min^{-1} with CdSQDs/rGO-*TNAs, compared to 2.30×10^{-4} min^{-1} with * TNAs and 6.25×10^{-4} min^{-1} with CdSQDs-*TNAs, signifying the role of rGO in the composite [142].

Energy storage

Fast charging devices are a necessity in today's society since the use of electronic devices have skyrocketed. Supercapacitors that exhibit long life cycles, fast charging and discharging process as well as larger

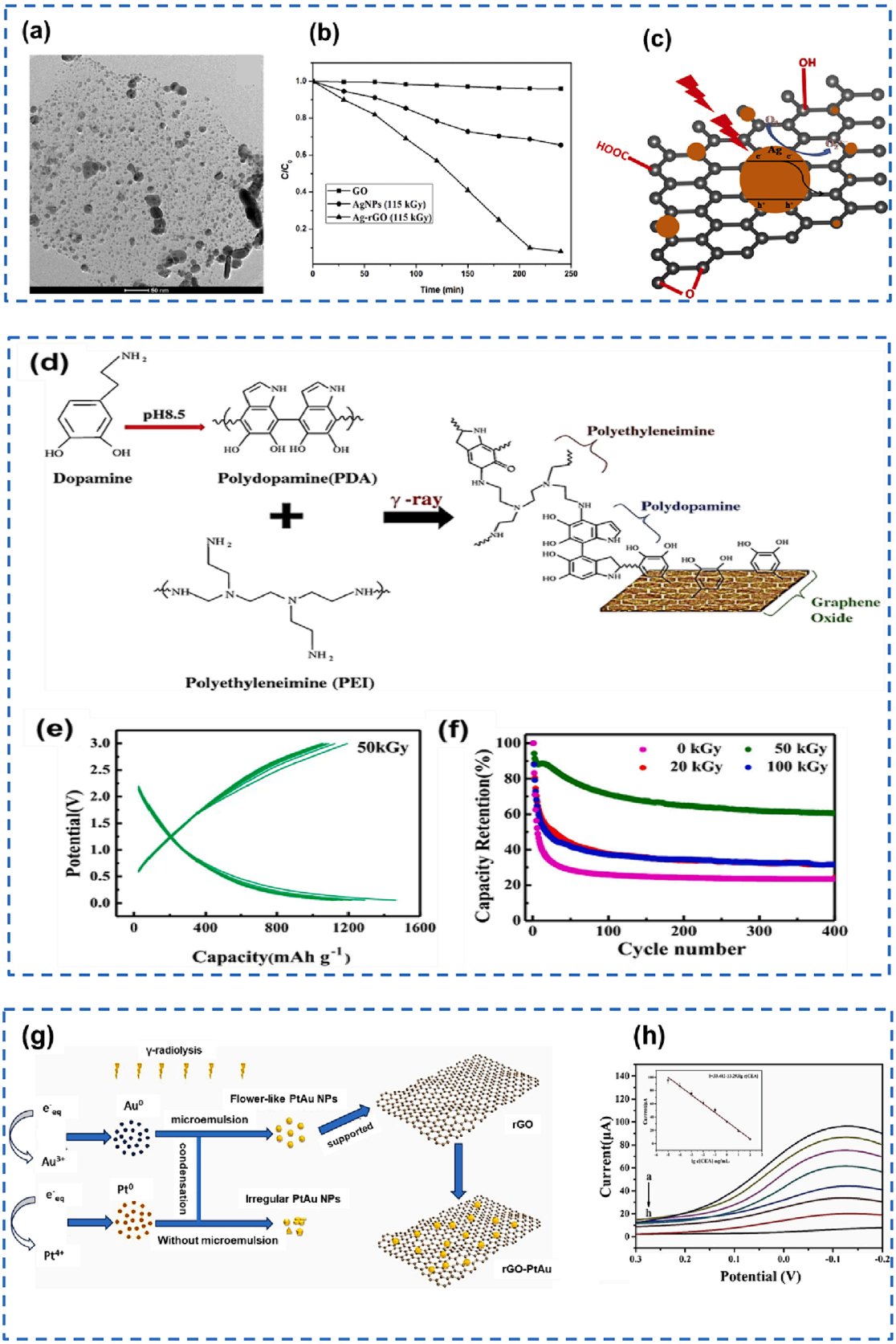

Fig. 10. (a) TEM micrograph showing uniformly distributed AgNPs on GO in the Ag-rGO formed by irradiation at 115 kGy, (b) Photocatalytic degradation kinetics of MB by GO, Ag and Ag-rGO where C_0 is initial concentration of MB solution and C is the MB concentration at time t, (c) Schematic of photocatalytic process taking place on the Ag-rGO under visible light irradiation for the degradation of MB. Reprinted with permission from ref. [152]. (d) Diagrammed presentation reaction mechanism of PDA for self-polymerization and formation of GO–PDA–PEI composites, (e) Galvanostatic charge/discharge profiles of GO–PDA–PEI composite electrodes at a current density of 1 A/gafter γ-ray irradiation of dose 50 kGy, (f) comparison of cycle performance of the GO–PDA–PEI composite electrodes up to 400

cycles at 1 A/g in accordance with the γ-ray irradiation of different doses. Reprinted with permission from ref. [165], (g) Schematic representation for the synthesis of rGO-PtAu by via gamma irradiation and microemulsion, (h) Square wave voltammetry plot of the immunosensor for different concentration of CEA, from a to h: 10 fg mL^{-1}, 100 fg·mL^{-1}, 1 pg·mL^{-1}, 10 pg·mL^{-1}, 100 pg·mL^{-1}, 1 ng mL^{-1}, 10 ng mL^{-1},100 ng mL^{-1}. Insert: calibration curves of immunosensor to different concentrations of CEA. Reprinted with permission from ref. [170], (i) XRD patterns of rGO and rGO-Sr obtained via gamma radiation, (j) High-resolution TEM micrograph of rGO-Sr, (k) antimicrobial activity of GO, rGO and rGO-Sr, (l) haemolytic activity of varying concentrations of GO, rGO and rGO-Sr. Reprinted with permission from ref. [179].

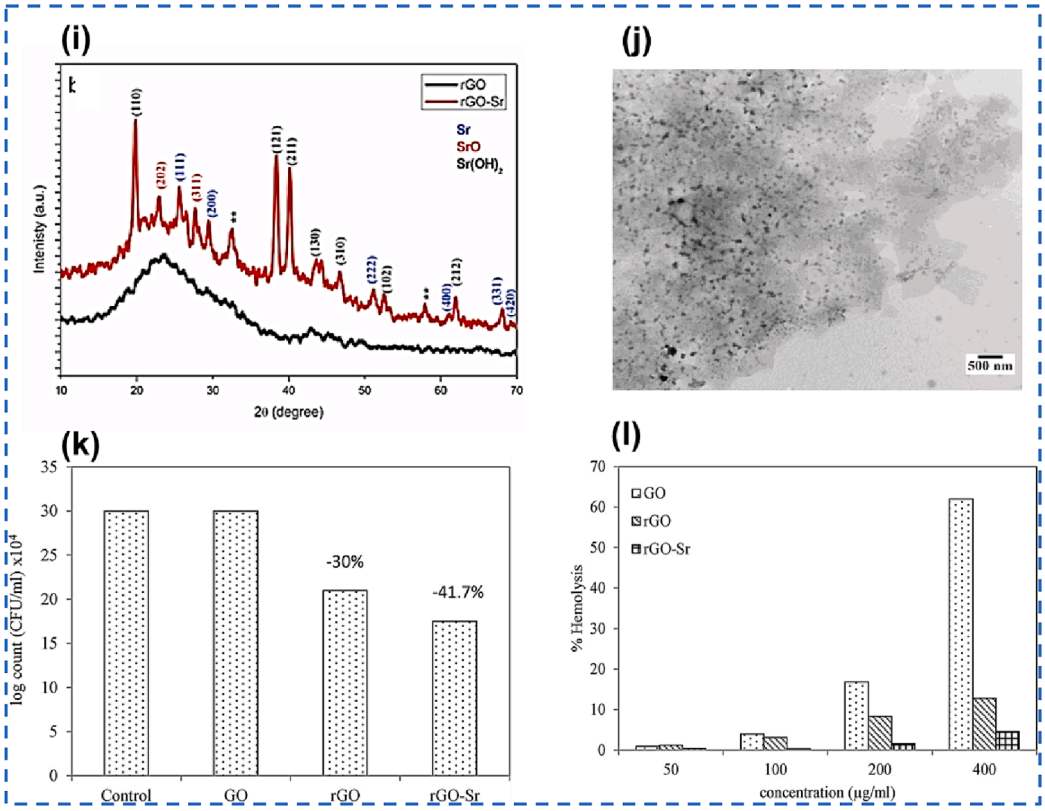

Fig. 10. (*continued*).

energy density compared to conventional capacitors are preferred and therefore in high demand [155]. Supercapacitors store energy either by forming an electric double layer near the interface of the electrode known as double layer capacitance or via a Faradic redox process as a result of charge transfer between the electrode and electrolyte [156]. An excellent supercapacitance electrode material must have a large surface area, and easily tuneable pore sizes. These materials include carbonaceous materials comprising of CNT, fullerenes, GO and rGO [157]. GBNMs are suitable candidates as an electrode material compared to other carbon-based materials due to high specific capacitance (~214 μF/cm^2), good cyclic ability and high-power density [158] and very high surface area to volume ratio [159]. However, due to agglomeration of graphene sheets the capacitance GBNMs is compromised. To alleviate this limitation, transition metal oxides, conducting polymer, metals and other carbon materials have been incorporated into graphene, diffusion of electrolyte in graphene sheets have been enhanced by using these various spacers, and lastly by irradiation treatment [157]. Among the methods used to synthesize graphene-based supercapacitors and batteries's electrodes is γ-radiolysis. Gr-Au nanocomposites produced by γ-irradiation and chemical synthesis revealed that the electrode whose catalyst was γ-synthesized had a specific capacitance value five times higher than that of the chemically synthesized electrode. Furthermore, the Gr-Au produced by γ-radiolysis had a lengthy cycle life, maintaining about 90 % of its capacitance even after 600 cycles [160]. Prior, PtNP decorated graphene for supercapacitors was synthesized via γ-ray irradiation at an optimal dose of 300 kGy at pH 12 labelled (PR-V). The PtNPs increased the C:O atomic ratio in rGO and repaired defects thereby enhancing the electron and ion transport migration which resulted in the improvement of specific capacitance (154F g^{-1}) at 0.1 A/g. The rate retention was 72.3 % at 20 A/g [161]. Atta et al. reported a novel, one-pot, and single-step method for synthesizing reduced graphene oxide/silver nanocomposites (rGO/Ags) with different Ag ratios using Roselle extract as a scavenger for oxidative free radicals and 80 kGy of γ-ray for symmetric supercapacitor applications. The Roselle extract inhibited the formation of the AgO phase but promoted the formation of uniformly dispersed Ag phase on rGO. The symmetric supercapacitor demonstrated good performance with low internal resistance and suitable specific capacitance (96 F g^{-1}at current density 0.2 A/g) [162].

Batteries are devices that convert chemical energy into electrical energy by means of an electrochemical oxidation reduction reaction [163]. They are classified into primary batteries and secondary batteries. While primary batteries are not rechargeable and have non-reversible electrochemical reactions, secondary batteries are rechargeable with reversible electrochemical reactions. All the batteries consist of an anode, cathode and electrolyte that completes the circuit when the system is connected. Due to rechargeability, secondary batteries comprising lithium-ion batteries (LIB) whose anode side is made of graphite and the cathode side is made of lithium metal oxide or lithium polymer are actively explored [164]. More lithium ions in the electrodes enhance the energy density of the batteries. The large surface area of graphene and its derivatives provides an active surface for adsorption of lithium ions by which more lithium ions are stored to make LIBs more efficient. In addition, graphene sheets boost the conductivity of lithium metal and hence the electrochemical performance of LIBs [164]. To enhance the cycle stability in Li-ion batteries Jo and colleagues modified

the structural stability of anode for these batteries through γ-ray irradiation of GO containing polydopamine (PDA) and polyethyleneimine (PEI) at different doses (0–100 kGy) as shown in Fig. 10d. The unradiated sample's first charging and discharging capacities were 203 and 792 mA h g^{-1}, respectively and the capacity of un-radiated composites decreased more than that of the γ-ray-irradiated samples in the second charging and discharging cycles. The optimally radiated sample (50 kGy) recorded a capacity of 1300 mA h g^{-1} (Fig. 10e) owing to the crosslinking and GO reduction induced by the γ-ray irradiation [165]. The optimal sample retained ~ 70 % capacitance after 400 cycles as shown in Fig. 10f. The results were better than those observed when "Janus"-structured nanocomposites were fabricated with Fe_3O_4 NPs and PDA on each side of GO nanosheet using the Langmuir–Schaefer technique [166]. Liang and Lu prepared Fe_3O_4/rGO nanocomposites with different weight concentration of Fe_3O_4 via γ-irradiation method to improve the anode electrode of LIB. The discharge/charge cycling stability of the composite was remarkedly improved in comparison with that of unmodified Fe_3O_4NPs. While the Fe_3O_4/rGO-2 composite (wt% of Fe_3O_4 ≈ 78.8 %) exhibited the highest cycling stability at a current density of 50 mA g^{-1} with a discharge capacity of 568.6 mAh/g after 100 cycles, the Fe_3O_4/rGO-3 (wt% of Fe_3O_4 ≈ 74.7 %) displayed an even better cycling stability at a higher current density (500 mA g^{-1}), that sustained a discharge capacity of 738.5 mAh/g after 100 cycles [108].

Sensing

A sensor is a device that detects physical input from its surroundings. This input could be any kind of physical phenomenon, such as motion, heat, light, pressure, or moisture [167]. Usually, the output is transmitted as a signal to a reader computer so that a human can analyze it. Noteworthy, among electrochemical-based sensors are graphene-based ones because of their greater flexibility, electrical conductivity, reduced electrical noise, and ease of use. For example, graphene-based sensors can detect hydrazine more easily than other carbonaceous materials because the metallic impurities in the former compromise the performance of the sensor. They also work well for the detection of biomolecules [168], and gas sensing [169]. Li and colleagues developed an extremely sensitive flower-like PtAu/rGO that served as a label-free immunosensor for the detection of carcinoma embryonic antigen (CEA) via microemulsion and γ-radiation as shown in Fig. 10g. The as-synthesized PtAu/rGO nanocomposites had an improved electrode surface area and offered a biocompatibility, durable matrix enabling simple conjugation of antibodies, ensuring a very efficient immunoassay platform. Fig. 10h shows that the redox current at −0.124 V of the immunosensor decreased with increasing concentration of CEA loaded on the electrode (rGO-PtAu/GCE). The insert in Fig. 10h demonstrate a linear relationship between the redox peak current and the logarithm of CEA concentration within the range 10 fg·mL^{-1} to 1 × 10^8 fg·mL^{-1} and a very low limit of detection (7 fg·mL^{-1}). Furthermore, the immunosensor exhibited superior specificity with the interference of other biological molecules [170]. A hydrogel patch was fabricated via γ-irradiation by crosslinking a solution of GO with poly acrylic acid and cellulose nanofiber. Owing to its high sorption ability and transparency, the hydrogel could be used for colorimetric detection of urea in sweat. When the quantity of urea increased, the colorimetric sensor clearly changed colour within a linear range of 40–80 mM, which covered 60 mM which is a cut-off value for the diagnosis of chronic kidney disease (CKD). When the hydrogel served as a substrate to directly quantify urea in sweat in laser desorption ionization mass spectroscopy (LDI-MS) it was found that GO promoted the laser desorption ionization of urea and significantly improved the functions of the hydrogel. Therefore, the hydrogel patch can potentially be used in non-invasive and dual detection of CKD in medical diagnosis [171].

The γ-radiolysis technique has also been used to prepare GBNMs for other analytes apart from biomolecules. For instance, γ-irradiation concurrently functionalized graphene quantum dots (GQDs) with amino groups and doped the dots with N atoms by irradiating GQDs in a water-IPA medium and EDA, at doses of 25, 50 and 200 kGy. Due to amino functionalization, the zeta potential of dots changed from − 34.6 to + 9.1 mV. The photoluminescence quantum yields (PLQY) were also elevated from 2.07 % for non −irradiated GQDs to 18.40 % for irradiated GQDs (200 kGy). The modified GQDs optically detected Cu(II) ions in water as a sensor. The data fitted the linear model of Stern-Volmer equation in the 0.3–6.4 μmol/L and 0.3–16.1 μmol/L ranges for pristine GQDs and modified GQDs 200 kGy, respectively, with limit of detection (LOD) of 0.187 nmol/L (R^2 = 0.974) and 153 nmol/L (R^2 = 0.984) for pristine GQDs and modified GQDs respectively [172]. The LOD values are comparable to literature [173].

Antimicrobial

An antimicrobial agent is a material that, as a result of physiological interactions damages organelles such as cell membranes, lipids, proteins, and DNA, to cause microbial cell death (bactericidal) or inhibits bacterial cell growth (bacteriostatic) [174]. Antibacterial properties in GBNMs are determined by the lateral size, shape and the number of layers since these influences the dispersibility, number of corners and sharp edges that are said to cut through the cell membrane of bacteria and cause leakage of the organelles and hence lysis [175,176]. The mechanism of action by GBNMs include nano knives action by the sharp edges [174], oxidative stress mediation with or without ROS, and lipid bilayer extraction among many [177]. For antimicrobial purporses strontium NPs decorated rGO (rGO-Sr) were prepared via γ-irradiation. The formation of rGO-Sr was confirmed by the XRD pattern (red curve) which displays the amorphous nature and broad peak of RGO at ~ 24° and peaks arising from SrO and SrOH respectively as shown in Fig. 10i. In Fig. 10j the TEM confirms uniform dispersion of the SrNPs on the rGO surface. The decoration of rGO sheets with SrNPs remarkably improved antibacterial activity of the composite against *Staphylococcus aureus* (*S. aureus*). The antibacterial results are comparable to those obtained by [178] who prepared graphene-Fe_3O_4 nanocomposites via the solvothermal method. In addition, rGO-Sr treated red blood cells had no signs of haemolysis at 50 and 100 μgmL^{-1}, while haemolysis of 1.6 % and 4.6 % at 200 and 400 μgmL^{-1} respectively was evident as displayed in Fig. 10k. The haemolysis of the composite is far less than that of unmodified GO and rGO due to the electrostatic repulsion between the positively charged Sr^{2+} ions and phosphatidylcholine groups present on the red blood cell membrane [179]. Poly (methyl methacrylate) (PMMA)-reduced graphene oxide (rGO) (PrGO) composite films were synthesized by solvent evaporation and exposed to γ-radiation at different dosages (25, 50 and 100 kGy). The PrGO50 and PrGO100 samples exhibited bigger zone of inhibition against *Escherichia coli* (*E. coli*) and were hemocompatible [116]. A novel synthesis of magnesium oxide nanoparticles (MgONPs) and GO/MgO nanocomposite was realised by using fermented *Erysiphe cichoracearum,* an agricultural by-product as a reductant. MgONPs were irradiated at 30 kGy while optimal GO/MgO nanocomposite was obtained at 20 kGy. The average size of MgONPs was 14.5 nm and homogenously spread of the GO sheets. The GO/MgO nanocomposite exhibited excellent antimicrobial efficacy with minimum inhibitory concentration (MIC) value of 25.0 μg/mL for *E. coli,* and 50.0 μg/mL for *Candida albicans* [180]. Chitosan (CS)/GO composite films were prepared by γ-ray irradiation at 10, 20, and 40 kGy. The tensile strength was enhanced at the lower dose (10 kGy) however it declined at elevated irradiation dosages (20–40 kGy). The composite demonstrated enhanced antibacterial activity against *Bacillus subtilis*, compared to *E. coli* and *S. aureus*. The optimal radiation dose for antibacterial activity was 20 KGy [181]. A monolithic PAM-GO-Ag hydrogel was prepared via γ-ray irradiation at 30 kGy. The hydrogel displayed ~ 90 % bactericidal activity that was achieved through cell membrane damage, protein leakage, and increased ROS mechanisms [182]. Hydrophobic carbon quantum dots/polyurethane nanocomposite (hCQD-PU) were prepared separately and later irradiated (1, 10, and

200 kGy) in air. The irradiated composites resulted into a rise in ROS production. The best antibacterial activity was observed at 200 kGy, with the complete eradication of *S. aureus* and *E. coli* after 15 min exposure to a blue light [183].

Cancer treatment modalities

The damage that conventional cancer treatment regimens like radiation therapy, chemotherapy, and surgery cause to normal tissue cells emphasizes the need for innovative strategies that will have fewer negative consequences on the patient's body. This has led to the exploration of nanomaterial-based photothermal therapy (PTT) [184], photodynamic therapy (PDT) [185] and bioimaging. PTT compounds are photothermal because they transform light into thermal energy. The concentration of the photothermal substance, the length of the light exposure, and the light's intensity can all be controlled to regulate the amount of heat that is produced [186]. This anticancer therapy is highly selective and specific to cancerous cells. Moreover, it can be used in conjunction with other therapeutic modalities to improve the course of treatment. PDT, on the other hand, is a two-step procedure that uses light energy, and a drug called a photosensitizer to kill cancer cells when they are activated by light at a particular wavelength, typically from a laser source. The photosensitizer is nontoxic until it is activated by light [185]. Ideal nanomaterials for this application must fluoresce in the near infrared (NIR) for deep tissue penetration and traceability, must be photothermal, and be nontoxic. Among the explored nanomaterials for PTT, PDT and bioimaging are AuNPs [187] conventional and tertiary QDs [185] and graphene quantum dots (GQDTs). Besides exhibiting tuneable optical properties, GQDTs are biocompatible and less toxic [188]. Owing to their enormous surface area and inherent two-dimensionality, GO and rGO sheets are frequently used as support materials to prevent the 0D and 1D materials from aggregating.

To investigate the effect of γ-irradiation dose on PTT efficiency of GO-Au, radiation doses (1–20 kGy) were applied to obtain AuNPs anchored onto GO sheets. The radiation concurrently reduced and uniformly distributed Au NPs on surface of GO that was also reduced GO and partially restored. The photothermal efficiency of the samples increased with an increase in radiation dose. The enhancement in the photothermal efficiency of the composite was ascribed to the degree of change in the size of AuNPs as well as reduction of GO caused by γ-radiation at different doses [189]. The same group had previously used electrochemically exfoliated graphene as a support to anchor AuNP that were prepared by the reduction of chloroauric acid under γ-irradiation at low doses of 1, 5, and 10 kGy. The average size of the attained AuNPs decreased with an increase in the applied dose. Upon being irradiated with 808 nm continuous wave laser for 10 min the samples showed an increase in temperature between 21.5 and 25.6 °C. The highest photothermal efficiency (73.55 %) was recorded at the lowest dosage (1 kGy) which indicated the potential application of that AuNPs-graphene composite in PTT [190]. Similar observations were made when GQDs were exposed with varying radiation doses. All radiation dosages enhanced the QDs' photoluminescence characteristics, however the GQDs exposed to lower doses of radiation had superior photoproduction capabilities compared to those exposed to higher levels. This implies that the structural alteration that result from irradiation have a direct impact on GQDs ability to produce singlet oxygen and their photostability under prolonged UV illumination. Therefore, low-dose irradiated GQDs are potential candidates for PDT [191].

Other applications of γ produced graphene composites

A concurrent formation of Co_3O_4 and reduction of GO was realized by [192] at 5.1 KGy/h for water splitting purposes. The rGO proved to be a viable medium for electron transfer which was confirmed by the photo-assisted H_2 generation studies that produced 3 and 30 $\mu molh^{-1}g^{-1}$ of H_2 for Co_3O_4 and Co_3O_4-rGO respectively. In a different study, GO supported cobalt oxyhydroxide nanoparticles (CoOOH NPs) were synthesized via a one-pot γ-radiolysis method to function as oxygen reduction reaction (ORR) catalyst for fuel cells at doses 25, 50 and 100 kGy. The electrocatalyst prepared with the 0.1 M Co precursor and exposed to 25 kGy displayed an excellent oxygen reduction activity due to the even distribution of high density CoOOH NPs on the surface of GO. The electrocatalyst displayed a 4 e^- transfer route in ORR with a low peroxide production (7.08 %). Although the ORR results obtained were improved the efficiency was still below that of commercial Pt/C catalyst [193]. A noble-metal-free ORR electrocatalyst (Fe/N-rGO) composite with varying Fe loadings (10 % to 20 %) was prepared by [82]. The field emission scanning electron microscopy (FESEM) revealed the presence of few FeNPs on the crumpled rGO surface. Linear sweep voltammetry performed with a rotating disk electrode in 0.1 M KOH in correspondence with electron transfer numbers were investigated with a Koutecky–Levich model indicated that the number of electrons transfers of the Fe/N-rGO composites was ~ 2. The finding suggest that the composites follow a 2 e^- transfer mechanism that has H_2O_2 as an intermediate product.

Challenges and future perspectives

Despite the undeniable progress in the modification of graphene via the γ-radiation technique in recent years, the technique still faces considerable problems that must be solved before it can be applied at an industrial scale. Some of the key challenges are:

- Even though radiolysis is a viable technology for mass production of GBNMs, the reaction chamber has limited irradiation space, smaller radiation sources as well as slow processing speed. To be at a commercial scale, bigger reaction volumes with high-speed processing time are required. New research that is focused on creating novel radiation sources that are bigger and safe can enhance the efficacy and sustainability of radiolysis for practical application of this technology in nanomaterials modification.
- While the γ-assisted synthesis of GBNMs is sustainable compared to other conventional synthesis methods, at very high dose rate and exposure time, the γ-radiolysis technique become affected by the decay of the γ-ray source (^{137}Cs or ^{60}Co) which may pose a risk to living organism in particular humans and the ecology at large [98]. This therefore requires that the γ-irradiation produced GBNMs toxicity be thoroughly investigated not only *in-vitro* but also *in-vivo* to gather a holistic idea on the extent or absence of toxicity that γ-irradiation synthesized GBNMs might have on living organisms as they may differ from conventional methods.
- Above the optimal dosage in the case of graphene-polymer composites the morphology is destroyed whereby in as much as the polymer is crosslinked it simultaneously undergo chain scission [165]. Once the chain scission occurs, the inorganic nanomaterial gets released from the matrix, causing aggregation of the nanomaterial thereby reducing the available surface area for activity depending on the application of the composite. Apart from the aggregation setback, the release nanomaterials also changes the durface charge of the composites, further compromising its efficiency towards the intended use.This underscores the need to strike a dose balance that is sufficiently enough to simultaneously modify the inorganic materials (graphene) and crosslink the polymer without inducing polymer chain scission.
- Apart from not being easily accessible, due to their danger that gamma rays can cause to the human body, the requirement of special environments like N_2, and or H_2 gases, alcohols etc, make this method not suitable for mass production of graphene-based devices.
- Understanding the structure and chemistry of the as-synthesized GBNMs and the various reducing agents through determining the optimal operational and reaction parameters for GBNMs for specific applications is the next crucial step. Exploration of strong natural

reducing agents like plant extracts could be tested in the production of doped and decorated reduced graphene composites instead of alcohols and probably even eliminating the requirements of inert atmosphere could be a major research focus that can promote the application of the technology in synthesis of reduced graphene composites.

- Although literature insinuates that the yield and the reduction degree of the graphene and its composites are lower in comparison to that obtained via chemical, laser-assisted, and thermal reduction methods [29]. A thorough process cost comparisons between the γ-ray assisted production and modification of GBNMs against conventionally synthesized materials should be made in the respective synthesis methods. However, this exercise is difficult to perform since in most reports on gamma radiolysis induced syntheses, the operational and reaction parameters are not optimised. Therefore, there is a need to optimise the reaction parameters per nanomaterial for specific application. Considering this, modelling and simulation of this technique should be intensely explored for a deeper comprehension of the synthesis mechanisms and parameters that influence the characteristics of respective GBNMs. Mastery of such information may assist in speeding up commercialization of this technique. Additionally, research should focus on standardization and quality control of GBNMs produced using γ-irradiation method, as it produces materials with unique structures, physical, chemical, and electrical properties.

Conclusions and prospects

This review provides succinct overview of γ-radiation assisted modification of graphene-based nanomaterials (GBNMs). The modifications discussed include reduction, etching, doping, functionalization, and formation of graphene-based composites. The conditions needed as well as the mechanisms behind the respective modifications are also presented. The key reaction and operational parameters that significantly affect the structural properties and hance applicability of these materials *viz* pH, irradiation dose and rate, as well as the source of radicals are discussed. Graphene-based nanocomposites have superior electrical conductivity, high specific surface area, and outstanding stability, making them ideal for applications such as energy storage, sensors, catalysis and biomedical. Fabrication of graphene nanocomposites like metal-graphene, metal oxide-graphene, graphene-carbon nanotubes via gamma radiation has shown to enhance the performance of graphene as does conventional methods. Besides operating at room temperature which saves a lot of energy, the other major advantage of γ-radiation synthesis is the ease of controlling the reaction parameters such as radiation dose, time, and rate to manipulate the size, crystallinity and structure of the nanomaterials [29]. The controllability of the reaction process also enables researchers to draw conclusions on the point of transformation. The challenges and future perspective section highlight research gaps that exist in γ-radiation synthesis of GBNMs hindering their various applications at commercial level. To close the research gaps, full comprehension of the structure and optimisation of all the radiolysis parameters involved in preparing individual GBNMs for specific applications must be reached. Moreover, deep investigation of the toxicity of the as-prepared materials is necessary prior to full blown industrialisation of the technique.

Radiolysis assisted production of nanomaterials has a promising future as researchers continually investigate its prospects and refine its settings for enhanced effectiveness and scalability. Currently biocompatible graphene composites have a wide applicability such as in biomedical applications. Due to capability of γ-irradiation approach to produce acceptable yields this method is a potential alternative to the production of GBNMs to be use in heat management and family of coolants where GBNMs are often dispersed in matrices such as water and ethylene glycol to enhance thermal conductivities in nanofluids [124,125]. These GBNMs however are synthesized via other means except γ-radiolysis. Therefore, gamma irradiation produced GBNMs still have a greater chance in this field as demonstrated by [126]. Compared to other nano-fluid synthesis methods, radiolysis needs no vacuum. Another research field that is gaining traction is fabrication of complex nanostructures with numerous components. As such, core–shell nanocomposites with a metallic core and a semiconductor (including graphene) shell with potential application in solar cells and photocatalysis have been realized. Radiolysis can potentially revolutionise nanocomposite synthesis and create new prospects for its usage in a variety of industries but that is contingent on the technology's commercial feasibility.

Funding

This research received funding from South African Coal, Oil, and Gas Corporation-National Research Foundation (SASOL-NRF) University Collaborative Research Grants (Grant No. 138626) and Reference (SASOL800405).

CRediT authorship contribution statement

Nkosingiphile E. Zikalala: Writing – original draft, Conceptualization, Writing – review & editing. **Shohreh Azizi:** Funding acquisition, Supervision, Conceptualization, Writing – review & editing. **Force T. Thema:** Writing – review & editing. **Karen J. Cloete:** Writing – review & editing. **Ali.A. Zinatizadeh:** Supervision, Visualization, Writing – review & editing. **Touhami Mokrani:** Visualization, Writing – review & editing. **Nomvano Mketo:** Writing – review & editing. **Malik M. Maaza:** Writing – review & editing.

Declaration of competing interest

The authors declare the following financial interests/personal relationships which may be considered as potential competing interests: Shohreh Azizi reports was provided by SASOL-NRF. Shohreh Azizi reports a relationship with National Research Foundation that includes: funding grants. If there are other authors, they declare that they have no known competing financial interests or personal relationships that could have appeared to influence the work reported in this paper.

Data availability

Data will be made available on request.

Acknowledgements

The UNESCO-Unisa Africa Chair for Nanoscience & Nanotechnology and SASOL-NRF University Collaborative Research Grants (Grant No.138626) and Reference (SASOL800405) are acknowledged as sources of support for the authors.

References

[1] N.A. Devi, S. Sinha, W.I. Singh, Silver-decorated reduced graphene oxide nanocomposite for supercapacitor electrode application, Bull. Mater. Sci. 45 (2022) 1–11, https://doi.org/10.1007/s12034-021-02583-3.
[2] Editorial, All in the graphene family – A recommended nomenclature for two-dimensional carbon materials, Carbon N. Y. 65 (2013) 1–6. 10.1016/j.carbon.2013.08.038.
[3] G. Yang, L. Li, W.B. Lee, M.C. Ng, Structure of graphene and its disorders : a review, Sci. Technol. Adv. Mater. 19 (2018) 613–648, https://doi.org/10.1080/14686996.2018.1494493.
[4] W. Nabgan, A. Abdul, B. Nabgan, M. Ikram, M. Wijayanuddin, P. Lakshminarayana, A state of the art overview of carbon-based composites applications for detecting and eliminating pharmaceuticals containing wastewater, Chemosphere. 288 (2022) 132535, https://doi.org/10.1016/j.chemosphere.2021.132535.
[5] S.-A. Rocio, F.J. Cano, P.J. Sebastian, O. Reyes-vallejo, Microwave-assisted biosynthesis of ZnO-GO particles using orange peel extract for photocatalytic

degradation of methylene blue, J. Environ. Chem. Eng. 10 (2022) 108924, https://doi.org/10.1016/j.jece.2022.108924.
[6] P. Li, X. Li, J. Huang, W. Qu, X. Pan, Q. Chen, Nitrogen-doped graphene oxide with enhanced bioelectricity generation from microbial fuel cells for marine sewage treatment, J. Clean. Prod. 376 (2022) 134071, https://doi.org/10.1016/j.jclepro.2022.134071.
[7] B.P. Tarasov, A.A. Arbuzov, A.A. Volodin, P.V. Fursikov, Metal hydride – Graphene composites for hydrogen based energy storage, J. Alloys Compd. 896 (2022) 162881, https://doi.org/10.1016/j.jallcom.2021.162881.
[8] K. Yokwana, A.T. Kuvarega, S.D. Mhlanga, E.N. Nxumalo, Mechanistic aspects for the removal of Congo red dye from aqueous media through adsorption over N-doped graphene oxide nanoadsorbents prepared from graphite flakes and powders, Phys. Chem. Earth. 107 (2018) 58–70, https://doi.org/10.1016/j.pce.2018.08.001.
[9] A. Ali, C. Hu, S. Jahan, B. Yuan, M.S. Saleh, E. Ju, S. Gao, R. Panat, Sensing of COVID-19 Antibodies in Seconds via Aerosol Jet Nanoprinted Reduced-Graphene-Oxide-Coated 3D Electrodes, Adv. Mater. 33 (2021) 1–15, https://doi.org/10.1002/adma.202006647.
[10] N. Ks, G. Ak, M. Sv, J. d, z. y, d. sv, g. iv, f. aa,, Electric Field Effect in Atomically Thin Carbon Films, Reports. 306 (2004) 666–669.
[11] K.A. Ritter, J.W. Lyding, Characterization of nanometer-sized, mechanically exfoliated graphene on the H-passivated Si (100) surface using scanning tunneling microscopy, Nanotechnology (2008) 015704, https://doi.org/10.1088/0957-4484/19/01/015704.
[12] S. Azizighannad, S. Mitra, Stepwise Reduction of Graphene Oxide (GO) and Its Effects on Chemical and Colloidal Properties, Sci. Rep. 8 (2018) 10083 |. 10.1038/s41598-018-28353-6.
[13] R. Wijaya, G. Andersan, S. Per, W. Irawaty, Green Reduction of Graphene Oxide using Kaffir Lime Peel Extract (Citrus hystrix) and Its Application as Adsorbent for Methylene Blue, Sci. Rep. 10 (2020) 1–9, https://doi.org/10.1038/s41598-020-57433-9.
[14] V. Gupta, N. Sharma, U. Singh, M. Arif, A. Singh, Higher oxidation level in graphene oxide, Optik (stuttg). 143 (2017) 115–124, https://doi.org/10.1016/j.ijleo.2017.05.100.
[15] V. Singh, D. Joung, L. Zhai, S. Das, S.I. Khondaker, S. Seal, Graphene based materials: Past, present and future, Prog. Mater. Sci. 56 (2011) 1178–1271, https://doi.org/10.1016/j.pmatsci.2011.03.003.
[16] R. Kumar, S. Sahoo, E. Joanni, R. Pandey, J.J. Shim, Vacancy designed 2D materials for electrodes in energy storage devices, Chem. Commun. 59 (2023) 6109–6127, https://doi.org/10.1039/d3cc00815k.
[17] A.E.D. Mahmoud, N. El-Maghrabi, M. Hosny, M. Fawzy, Biogenic synthesis of reduced graphene oxide from Ziziphus spina-christi (Christ's thorn jujube) extracts for catalytic, antimicrobial, and antioxidant potentialities, Environ. Sci. Pollut. Res. 29 (2022) 89772–89787, https://doi.org/10.1007/s11356-022-21871-x.
[18] S.M. Youssry, M.A. Elkodous, R. Kumar, G. Kawamura, W.K. Tan, A. Matsuda, Thermal-assisted synthesis of reduced graphene oxide-embedded Ni nanoparticles as high-performance electrode material for supercapacitor, Electrochim. Acta. 463 (2023) 142814, https://doi.org/10.1016/j.electacta.2023.142814.
[19] D. Losic, F. Farivar, P.L. Yap, T.T. Tung, M.J. Nine, New insights on energetic properties of graphene oxide (GO) materials and their safety and environmental risks, Sci. Total Environ. 848 (2022) 157743, https://doi.org/10.1016/j.scitotenv.2022.157743.
[20] Z. Ismail, Green reduction of graphene oxide by plant extracts : A short review, Ceram. Int. 45 (2019) 23857–23868, https://doi.org/10.1016/j.ceramint.2019.08.114.
[21] H. Guo, M. Peng, Z. Zhu, L. Sun, Preparation of reduced graphene oxide by infrared irradiation induced photothermal reduction, Nanoscale. 5 (2013) 9040–9048, https://doi.org/10.1039/c3nr02805d.
[22] S. Yong, K. Shyuan, S. Kartom, W. Ramli, W. Daud, Graphene production via electrochemical reduction of graphene oxide : Synthesis and characterisation, Chem. Eng. J. 251 (2014) 422–434, https://doi.org/10.1016/j.cej.2014.04.004.
[23] W. Wang, Y. Wu, Z. Jiang, M. Wang, Q. Wu, X. Zhou, Self-assembly of graphene oxide nanosheets in t-butanol/water medium under gamma-ray radiation, Chinese Chem. Lett. 29 (2018) 931–934, https://doi.org/10.1016/j.cclet.2017.11.003.
[24] R. Kumar, S. Sahoo, E. Joanni, R.K. Singh, K.K. Kar, Microwave as a Tool for Synthesis of Carbon-Based Electrodes for Energy Storage, ACS Appl. Mater. Interfaces. 14 (2022) 20306–20325, https://doi.org/10.1021/acsami.1c15934.
[25] R. Kumar, S. Sahoo, E. Joanni, R. Pandey, W.K. Tan, G. Kawamura, S. A. Moshkalev, A. Matsuda, Microwave-assisted dry synthesis of hybrid electrode materials for supercapacitors: Nitrogen-doped rGO with homogeneously dispersed CoO nanocrystals, J. Energy Storage. 68 (2023) 107820, https://doi.org/10.1016/j.est.2023.107820.
[26] X. Li, H. Ren, X. Chen, J. Liu, Q. Li, C. Li, G. Xue, J. Jia, L. Cao, A. Sahu, B. Hu, Y. Wang, G. Jin, M. Gu, Athermally photoreduced graphene oxides for three-dimensional holographic images, Nat. Commun. 6 (2015), https://doi.org/10.1038/ncomms7984.
[27] X. Liu, L. Pan, Q. Zhao, T. Lv, G. Zhu, T. Chen, T. Lu, Z. Sun, C. Sun, UV-assisted photocatalytic synthesis of ZnO-reduced graphene oxide composites with enhanced photocatalytic activity in reduction of Cr(VI), Chem. Eng. J. 183 (2012) 238–243, https://doi.org/10.1016/j.cej.2011.12.068.
[28] F.T. Thema, P. Beukes, Z.Y. Nuru, L. Kotsedi, M. Khenfouch, M.S. Dhlamini, Physical properties of graphene via γ-radiolysis of exfoliated graphene oxide, Mater. Today Proc. 2 (2015) 4038–4045, https://doi.org/10.1016/j.matpr.2015.08.033.
[29] T.T. Tung, A.L.C. Pereira, E. Poloni, M.N. Dang, J. Wang, T.S.D. Le, Y.J. Kim, Q. H. Pho, M.J. Nine, C.J. Shearer, V. Hessel, D. Losic, Irradiation methods for engineering of graphene related two-dimensional materials, Appl. Phys. Rev. 10 (2023), https://doi.org/10.1063/5.0148376.
[30] A.M. Schwenke, S. Hoeppener, U.S. Schubert, Synthesis and Modification of Carbon Nanomaterials utilizing Microwave Heating, Adv. Mater. 27 (2015) 4113–4141, https://doi.org/10.1002/adma.201500472.
[31] Z. González, B. Acevedo, G. Predeanu, S.M. Axinte, M.F. Drăgoescu, V. Slăvescu, J.J. Fernandez, M. Granda, G. Gryglewicz, S. Melendi-Espina, Graphene materials from microwave-derived carbon precursors, Fuel Process. Technol. 217 (2021), https://doi.org/10.1016/j.fuproc.2021.106803.
[32] G. Yasin, S. Ibrahim, S. Ajmal, S. Ibraheem, S. Ali, A.K. Nadda, G. Zhang, J. Kaur, T. Maiyalagan, R.K. Gupta, A. Kumar, Tailoring of electrocatalyst interactions at interfacial level to benchmark the oxygen reduction reaction, Coord. Chem. Rev. 469 (2022) 214669, https://doi.org/10.1016/j.ccr.2022.214669.
[33] N. Singh, Radioisotopes-Application in physical sciences, 1st ed., InTech, Janeza Trdine, 2011.
[34] S.M. Majhi, A. Mirzaei, S. Navale, H.W. Kim, S.S. Kim, Boosting the sensing properties of resistive-based gas sensors by irradiation techniques: A review, Nanoscale. 13 (2021) 4728–4757, https://doi.org/10.1039/d0nr08448d.
[35] X. Xie, Y. Zhou, K. Huang, Advances in microwave-assisted production of reduced graphene oxide, Front. Chem. 7 (2019) 1–11, https://doi.org/10.3389/fchem.2019.00355.
[36] Y. Han, C. Guo, P. Liu, N. Li, C. Min, B. Zhu, H. Shi, X. Pei, Z. Xu, Applied Surface Science Graphene oxide membranes with short-range pore channels toward ultrafast water transport via γ-ray etching, Appl. Surf. Sci. 608 (2023) 155150, https://doi.org/10.1016/j.apsusc.2022.155150.
[37] Z. Xu, L. Chen, B. Zhou, Y. Li, B. Li, J. Niu, M. Shan, Q. Guo, Z. Wang, X. Qian, Nano-structure and property transformations of carbon systems under γ-ray irradiation: A review, RSC Adv. 3 (2013) 10579–10597, https://doi.org/10.1039/c3ra00154g.
[38] S. Majid, S. Kang, G.S. Rama, M. Norouzi, γ-Radiolysis as a highly efficient green approach to the synthesis of metal nanoclusters : A review of mechanisms and applications, Chem. Eng. J. 360 (2019) 1390–1406, https://doi.org/10.1016/j.cej.2018.10.164.
[39] G.G. Flores-Rojas, F. Lopez-Saucedo, E. Bucio, Gamma-irradiation applied in the synthesis of metallic and organic nanoparticles : A short review, Radiat. Phys. Chem. 169 (2018) 107962, https://doi.org/10.1016/j.radphyschem.2018.08.011.
[40] M.J. Saif, M. Naveed, R. Akhtar, Irradiation applications for polymer nano-composites : A state-of-the-art review, J. Ind. Eng. Chem. 60 (2018) 218–236, https://doi.org/10.1016/j.jiec.2017.11.009.
[41] L. Shahriary, A.A. Athawale, Synthesis of graphene using gamma radiations, Bull. Mater. Sci. 38 (2015) 739–745.
[42] L.M. Alrehaily, J.M. Joseph, M.C. Biesinger, D.A. Guzonas, J.C. Wren, Gamma-radiolysis-assisted cobalt oxide nanoparticle formation, Phys. Chem. Chem. Phys. 15 (2013) 1014–1024, https://doi.org/10.1039/c2cp43094k.
[43] S. Ahmad, R. Hammad, S. Rubab, Gamma Radiation-Induced Synthesis of Polyaniline - Based Nanoparticles/Nanocomposites, J. Electron. Mater. 51 (2022) 5550–5567, https://doi.org/10.1007/s11664-022-09823-0.
[44] Y. He, J. Li, L. Li, J. Li, Gamma-ray irradiation-induced reduction and self-assembly of graphene oxide into three-dimensional graphene aerogel, Mater. Lett. 177 (2016) 76–79, https://doi.org/10.1016/j.matlet.2016.04.187.
[45] W. Wang, Y. Wu, Z. Jiang, M. Wang, Q. Wu, X. Zhou, X. Ge, Formation mechanism of 3D macroporous graphene aerogel in alcohol-water media under gamma-ray radiation, Appl. Surf. Sci. 427 (2018) 1144–1151, https://doi.org/10.1016/j.apsusc.2017.09.058.
[46] Y. He, J.L.L. Li, J.C.J. Li, The synergy reduction and self-assembly of graphene oxide via gamma-ray irradiation in an ethanediamine aqueous solution, Nucl. Sci. Tech. 27 (2016) 1–8, https://doi.org/10.1007/s41365-016-0068-8.
[47] L.F. Dumée, C. Feng, L. He, F. Allioux, Z. Yi, W. Gao, C. Banos, J.B. Davies, L. Kong, Tuning the grade of graphene: Gamma ray irradiation of free-standing graphene oxide films in gaseous phase, Appl. Surf. Sci. J. 322 (2014) 126–135, https://doi.org/10.1016/j.apsusc.2014.10.070.
[48] A. Guirguis, J.W. Maina, L. Kong, L.C. Henderson, A. Rana, L. Hua, M. Majumder, L.F. Dum, Perforation routes towards practical nano-porous graphene and analogous materials engineering, Carbon n. y. 155 (2019) 660–673, https://doi.org/10.1016/j.carbon.2019.09.028.
[49] C. Yu, B. Zhang, F. Yan, J. Zhao, J. Li, L. Li, Engineering nano-porous graphene oxide by hydroxyl radicals, Carbon n. y. 105 (2019) 291–296, https://doi.org/10.1016/j.carbon.2016.04.050.
[50] Y. Zhang, L. Chen, Z. Xu, Y. Li, B. Zhou, M. Shan, Z. Wang, Preparing graphene with notched edges and nanopore defects by γ-ray etching of graphite oxide, Mater. Lett. 89 (2012) 226–228, https://doi.org/10.1016/j.matlet.2012.08.113.
[51] D.F. Ludovic, C. Feng, L. He, Z. Yi, F. She, Z. Peng, W. Gao, C. Banos, J.B. Davies, C. Huynh, S. Hawkins, M.C. Duke, S. Gray, P.D. Hodgson, L. Kong, Single step preparation of meso-porous and reduced graphene oxide by gamma-ray irradiation in gaseous phase, Carbon n. y. 70 (2014) 313–318, https://doi.org/10.1016/j.carbon.2013.12.094.
[52] Y. Han, C. Guo, P. Liu, N. Li, C. Min, B. Zhu, H. Shi, X. Pei, Z. Xu, Graphene oxide membranes with short-range pore channels toward ultrafast water transport via γ-ray etching, Appl. Surf. Sci. 608 (2023) 155150, https://doi.org/10.1016/j.apsusc.2022.155150.
[53] C. Tyagi, A. Tripathi, A. Bikash, D.K. Avasthi, Structural changes induced in graphene oxide film by low energy ion beam irradiation, Radiat. Phys. Chem. 192 (2022) 109923, https://doi.org/10.1016/j.radphyschem.2021.109923.

[54] S. Pei, H. Cheng, The reduction of graphene oxide, Carbon n. y. 50 (2011) 3210–3228, https://doi.org/10.1016/j.carbon.2011.11.010.
[55] M.M. Atta, H.A. Ashry, G.M. Nasr, H.A.A. El-rehim, Electrical, thermal and electrochemical properties of γ-ray-reduced graphene oxide, Int. J. Miner., Metall. Mater. 28 (2021) 1726–1734, https://doi.org/10.1007/s12613-020-2146-5.
[56] Z. Bowu, Z. Yujie, P. Cheng, Y. Ming, L. Linfan, D. Bo, H. Pengfei, F. Chanhai, L. Jingye, H. Qing, Preparation of polymer decorated Preparation of polymer decorated graphene oxide by γ-ray induced graft polymerization, Nanoscale. 4 (2012) 1742–1748, https://doi.org/10.1039/c2nr11724j.
[57] M.M. Atta, M.I.A.A. Maksoud, O.I. Sallam, A.S. Awed, Gamma irradiation synthesis of wearable supercapacitor based on reduced graphene oxide/cotton yarn electrode, J. Mater. Sci. Mater. Electron. 32 (2021) 3688–3698, https://doi.org/10.1007/s10854-020-05114-8.
[58] Z. Youwei, H. Ma, Z. Qilu, P. Jing, L. Jiuqiang, Z. Maolin, Y. Zhong-Zhen, Facile synthesis of well-dispersed graphene by γ-ray induced reduction of graphene oxide, J. Mater. Chem. 22 (2012) 13064–13069, https://doi.org/10.1039/c2jm32231e.
[59] M.M. Atta, M.E. Habieb, A. El, H. Mohamed, D.M. Lotfy, T.O. Eman, Radiation-assisted reduction of graphene oxide by aloe vera and ginger and their antioxidant and anti-inflammatory roles against male mice liver injury induced by gamma radiation, New J. Chem. 46 (2022) 4406–4420, https://doi.org/10.1039/d1nj05000a.
[60] T. Eman, H.A. Ashry, A. H, M.M. Atta, Gamma Radiation Assisted Green Reduction of Graphene Oxide by Doum Palm (Hyphaene Thebaica) Fruit Powder., Egypt. J. Chem. 65 (2022) 691–698. 10.21608/EJCHEM.2022.126667.5617.
[61] Z. Guo, S. Chakraborty, F.A. Monikh, D. Varsou, A.J. Chetwynd, A. Afantitis, I. Lynch, P. Zhang, Surface Functionalization of Graphene-Based Materials : Biological Behavior, Toxicology, and Safe-By-Design Aspects, Adv. Biol. 5 (2021) 2100637, https://doi.org/10.1002/adbi.202100637.
[62] A. Bonanni, C.K. Chua, M. Pumera, Rational Design of Carboxyl Groups Perpendicularly Attached to a Graphene Sheet : A Platform for Enhanced Biosensing Applications, Chem. a Eur. J. 20 (2014) 217–222, https://doi.org/10.1002/chem.201303582.
[63] J. Cho, I. Jeon, S.Y. Kim, S. Lim, J.Y. Jho, Improving Dispersion and Barrier Properties of Polyketone / Graphene Nanoplatelet Composites via Noncovalent Functionalization Using Aminopyrene, Appl. Mater. Interfaces. 9 (2017) 27984–27994, https://doi.org/10.1021/acsami.7b10474.
[64] M. Moschetta, J. Lee, J. Rodrigues, A. Podestà, O. Varvicchio, J. Son, Y. Lee, K. Kim, G. Lee, F. Benfenati, M. Bramini, A. Capasso, Hydrogenated Graphene Improves Neuronal Network Maturation and Excitatory Transmission, Adv. Biol. 5 (2021) 1–12, https://doi.org/10.1002/adbi.202000177.
[65] G. Chauhan, V. Chopra, A. Tyagi, G. Rath, "Gold nanoparticles composite-folic acid conjugated graphene oxide nanohybrids " for targeted chemo-thermal cancer ablation : In vitro screening and in vivo studies, Eur. J. Pharm. Sci. 96 (2017) 351–361, https://doi.org/10.1016/j.ejps.2016.10.011.
[66] M. Shi, T. Lin, M. Zhai, Functionalization of graphene oxide by radiation grafting polyhedral oligomeric silsesquioxane with improved thermal stability and hydrophilicity, J. Mater. Sci. 55 (2020) 1489–1498, https://doi.org/10.1007/s10853-019-04098-z.
[67] N.A. Daud, B.W. Chieng, N.A. Ibrahim, Z.A. Talib, E.N. Muhamad, Z.Z. Abidin, Functionalizing Graphene Oxide with Alkylamine by Gamma-ray Irradiation Method, Nanomaterials. 7 (2017) 1–15, https://doi.org/10.3390/nano7060135.
[68] K.M. Aujara, B.W. Chieng, N.A. Ibrahim, Gamma-Irradiation Induced Functionalization of Graphene Oxide with Organosilanes, Int. J. Melecular Sci. 20 (2019) 1910, https://doi.org/10.3390/ijms20081910.
[69] J. Wei, D. Zhou, Z. Sun, Y. Deng, Y. Xia, D. Zhao, A Controllable Synthesis of Rich Nitrogen-Doped Ordered Mesoporous Carbon for CO 2 Capture and Supercapacitors, Adv. Funct. Mater. 23 (2013) 2322–2328, https://doi.org/10.1002/adfm.201202764.
[70] R. Kumar, S. Sahoo, E. Joanni, R.K. Singh, K. Maegawa, W.K. Tan, G. Kawamura, K.K. Kar, A. Matsuda, Heteroatom doped graphene engineering for energy storage and conversion, Mater. Today. 39 (2020) 47–65, https://doi.org/10.1016/j.mattod.2020.04.010.
[71] R.K. Singh, R. Kumar, D.P. Singh, Graphene oxide: Strategies for synthesis, reduction and frontier applications, RSC Adv. 6 (2016) 64993–65011, https://doi.org/10.1039/c6ra07626b.
[72] K. Kakaei, G. Ghadimi, A green method for Nitrogen-doped graphene and its application for oxygen reduction reaction in alkaline media reduction reaction in alkaline media, Mater. Technol. 36 (2021) 46–53, https://doi.org/10.1080/10667857.2020.1724692.
[73] Q. Li, N. Mahmood, J. Zhu, Y. Hou, S. Sun, Graphene and its composites with nanoparticles for electrochemical energy applications, Nano Today. 9 (2014) 668–683, https://doi.org/10.1016/j.nantod.2014.09.002.
[74] C. Zhao, M. Zhang, Z. Liu, Y. Guo, Q. Zhang, Salt-Tolerant Superabsorbent Polymer with High Capacity of Water- Nutrient Retention Derived from Sulfamic Acid-Modi fi ed Starch, ACS Omega. 4 (2019) 5923–5930. 10.1021/acsomega.9b00486.
[75] K. Wu, Q. Liu, Applied Surface Science Nitrogen-doped mesoporous carbons for high performance supercapacitors, Appl. Surf. Sci. 379 (2016) 132–139, https://doi.org/10.1016/j.apsusc.2016.04.064.
[76] Y. Lu, S. Lo, J. Lin, W. Zhang, J. Lu, F. Liu, C. Tseng, Y. Lee, C. Liang, L. Li, Nitrogen-Doped Graphene Sheets Grown by Chemical Vapor Deposition : Synthesis and Influence of Nitrogen Impurities on Carrier Transport, ACS Nano. 7 (2013) 6522–6532, https://doi.org/10.1021/nn402102y.
[77] L.S. Panchakarla, K.S. Subrahmanyam, S.K. Saha, A. Govindaraj, H. R. Krishnamurthy, U.V. Waghmare, C.N.R. Rao, Synthesis, Structure, and Properties of Boron- and Nitrogen-Doped Graphene, Adv. Mater. 21 (2009) 4726–4730, https://doi.org/10.1002/adma.200901285.
[78] Y. Wang, Y. Shao, D.W. Matson, J. Li, Y. Lin, Nitrogen-Doped Graphene and Its Biosensing, ACS Nano. 4 (2010) 1790–1798, https://doi.org/10.1021/nn100315s.
[79] Z. Sheng, L. Shao, J. Chen, W. Bao, F. Wang, X. Xia, Catalyst-Free Synthesis of Nitrogen- Doped Graphene via Thermal Annealing Graphite Oxide with Melamine and Its Excellent Electrocatalysis, ACS Nano. 5 (2011) 4350–4358, https://doi.org/10.1021/nn103584t.
[80] Q. Liu, B. Guo, Z. Rao, B. Zhang, J.R. Gong, Strong Two-Photon-Induced Fluorescence from Photostable, Biocompatible Nitrogen-Doped Graphene Quantum Dots for Cellular and Deep-Tissue Imaging, Nano Lett. 13 (2013) 2436–2441, https://doi.org/10.1021/nl400368v.
[81] P. Kamedulski, S. Truszkowski, J.P. Lukaszewicz, Highly Effective Methods of Obtaining N-Doped Graphene by Gamma Irradiation, Materials (basel). 13 (2020) 4975, https://doi.org/10.3390/ma13214975.
[82] K.R. Rahman, K.Y. Kok, W.Y. Wong, H. Yang, Effect of Iron Loading on the Catalytic Activity of Fe/N-Doped Reduced Graphene Oxide Catalysts via Irradiation, Appl. Sci. 11 (2021) 1–10, https://doi.org/10.3390/app11010205.
[83] S. Yao, F. Jin, K. Yop, D. Hui, S. Park, Recent advances in carbon-fiber-reinforced thermoplastic composites : A review, Compos. Part B 142 (2018) 241–250, https://doi.org/10.1016/j.compositesb.2017.12.007.
[84] A. Tokai, K. Okitsu, F. Hori, Y. Mizukoshi, A. Iwase, One-step synthesis of graphene-Pt nanocomposites by gamma-ray irradiation, Radiat. Phys. Chem. 123 (2016) 68–72, https://doi.org/10.1016/j.radphyschem.2016.02.019.
[85] M.S. Umekar, R.G. Chaudhary, G.S. Bhusari, A. Mondal, A.K. Potbhare, S. Mahmood, Phytoreduced graphene oxide-titanium dioxide nanocomposites using Moringa oleifera stick extract, Mater. Today Proc. 29 (2020) 709–714, https://doi.org/10.1016/j.matpr.2020.04.169.
[86] X. Sun, C. Huang, L. Wang, L. Liang, Y. Cheng, W. Fei, Y. Li, Recent Progress in Graphene / Polymer Nanocomposites, Adv. Mater. 33 (2021) 2001105, https://doi.org/10.1002/adma.202001105.
[87] M. Cao, D.B. Xiong, L. Yang, S. Li, Y. Xie, Q. Guo, Z. Li, H. Adams, J. Gu, T. Fan, X. Zhang, D. Zhang, Ultrahigh Electrical Conductivity of Graphene Embedded in Metals, Adv. Funct. Mater. 29 (2019) 1–8, https://doi.org/10.1002/adfm.201806792.
[88] S. Ghosh, S. Bera, S. Bysakh, R.N. Basu, Highly Active Multimetallic Palladium Nanoalloys Embedded in Conducting Polymer as Anode Catalyst for Electrooxidation of Ethanol, Appl. Mater. Interfaces. 9 (2017) 33775–33790, https://doi.org/10.1021/acsami.7b08327.
[89] X. Zhao, N. Li, M. Jing, Y. Zhang, W. Wang, L. Liu, Z. Xu, L. Liu, F. Li, N. Wu, Monodispersed and spherical silver nanoparticles / graphene nanocomposites from gamma-ray assisted in-situ synthesis for nitrite electrochemical sensing, Electrochim. Acta. 295 (2019) 434–443, https://doi.org/10.1016/j.electacta.2018.10.039.
[90] J. Shi, W. Jiang, L. Liu, M. Jing, F. Li, Z. Xu, X. Zhang, Elucidating synthesis of noble metal nanoparticles/graphene oxide in free- scavenger γ-irradiation, Curr. Appl. Phys. 19 (2019) 780–786, https://doi.org/10.1016/j.cap.2019.03.022.
[91] D.P. Kepić, D.N. Kleut, Z.M. Marković, D.V. Bajuk-Bogdanović, V.B. Pavlovi, A.J. Krmpot, M.M. Lekic, D.J. Jovanović, B.M. Todorović-Marković, One-step preparation of gold nanoparticles - exfoliated graphene composite by gamma irradiation at low doses for photothermal therapy applications, Mater. Charact. 173 (2021) 110944. 10.1016/j.matchar.2021.110944.
[92] M. Lu, J. Li, S. Song, L. Li, J. Lin, The synthesis of 3D graphene/Au composites via γ-ray irradiation and their use for catalytic reduction of 4-nitrophenol, Nanotechnology. 31 (2020) 235604 (9pp). 10.1088/1361-6528/ab7aa5.
[93] F. Nurfiana, Giyatmi, N. Anggita, Synthesis of reduced graphene oxide modified Cu (rGO-Cu) by gamma irradiation and its electroactive properties, in: J. Phys. Conf. Ser., 20020: p. 012077. 10.1088/1742-6596/1436/1/012077.
[94] S. Joseph, O.N. Balasundaram, Effect of gamma radiation on structural, optical and electrical properties of ZnO thin films, Optoelectron. Adv. Mater. – RAPID Commun. 11 (2017) 377–380.
[95] A.M. Al-Baradi, A.A. Atta, A. Badawi, S.A. Algarni, A.S.A. Almalki, S.I. Ahmed, A. Ashour, A.S.A. Alsubaie, A.M. Hassanien, M.M. El-Nahass, Tailoring the optical properties of tin oxide thin films via gamma irradiation, Zeitschrift Fur Naturforsch. - Sect. A J. Phys. Sci. 76 (2021) 1133–1146, https://doi.org/10.1515/zna-2021-0215.
[96] R. Kajal, B.R. Kataria, K. Asokan, D. Mohan, Effects of gamma radiation on structural, optical, and electrical properties of SnO2 thin films, Appl. Surf. Sci. Adv. 15 (2023) 100406, https://doi.org/10.1016/j.apsadv.2023.100406.
[97] M.M. Mutter, H.K. Atty, A.A. Hateef, Influence of Gamma Radiation on Structural and Optical Properties of Fe_2O_3 Thin Films Prepared by Chemical Spray Technique, Int. Lett. Chem. Phys. Astron. 63 (2016) 22–28. 10.56431/p-530z5l.
[98] Z.S. Wu, G. Zhou, L.C. Yin, W. Ren, F. Li, H.M. Cheng, Graphene/metal oxide composite electrode materials for energy storage, Nano Energy. 1 (2012) 107–131, https://doi.org/10.1016/j.nanoen.2011.11.001.
[99] I.V. Lightcap, T.H. Kosel, P.V. Kamat, Anchoring semiconductor and metal nanoparticles on a two-dimensional catalyst mat. storing and shuttling electrons with reduced graphene oxide, Nano Lett. 10 (2010) 577–583, https://doi.org/10.1021/nl9035109.
[100] P.V. Kamat, Graphene-based nanoarchitectures. Anchoring semiconductor and metal nanoparticles on a two-dimensional carbon support, J. Phys. Chem. Lett. 1 (2010) 520–527, https://doi.org/10.1021/jz900265j.
[101] R. Kumar, R.K. Singh, D.P. Singh, R. Savu, S.A. Moshkalev, Microwave heating time dependent synthesis of various dimensional graphene oxide supported

hierarchical ZnO nanostructures and its photoluminescence studies, Mater. Des. 111 (2016) 291–300, https://doi.org/10.1016/j.matdes.2016.09.018.
[102] C. Casiraghi, Probing disorder and charged impurities in graphene by Raman spectroscopy, Phys. Status Solidi - Rapid Res. Lett. 3 (2009) 175–177, https://doi.org/10.1002/pssr.200903135.
[103] B. Gupta, A.A. Melvin, T. Matthews, S. Dhara, S. Dash, A.K. Tyagi, Facile gamma radiolytic methodology for TiO2-rGO synthesis : Effect on photo-catalytic H2 evolution, Int. J. Hydrogen Energy. 40 (2015) 5815–5823, https://doi.org/10.1016/j.ijhydene.2015.02.102.
[104] X. Xie, L. Li, S. Ye, Q. Zhang, X. Chen, X. Huang, Photocatalytic degradation of ethylene by TiO 2 nanotubes / reduced graphene oxide prepared by gamma irradiation, Radiat. Phys. Chem. 165 (2019) 108371, https://doi.org/10.1016/j.radphyschem.2019.108371.
[105] N. Azwen, N. Azmy, A. Ashrif, A. Bakar, N. Arsad, S. Idris, A. Rahman, A. Abdul, Enhancement of ZnO-rGO nanocomposite thin films by gamma radiation for E. coli sensor, Appl. Surf. Sci. 392 (2017) 1134–1143, https://doi.org/10.1016/j.apsusc.2016.09.144.
[106] I.K. Abbas, L.A. Najam, A.U. Auobsulaiman, The Effect of Gamma Irradiation on the Structural Properties of Porous Silicon, Int. J. Phys. 3 (2015) 1–7, https://doi.org/10.12691/ijp-3-1-1.
[107] X. Li, X. Zheng, J. Shao, T. Gao, Q. Shi, Q. Qu, Synergistic Ternary Composite (Carbon/Fe3O4@Graphene) with Hollow Microspherical and Robust Structure for Li-Ion Storage, Chem. - A Eur. J. 22 (2016) 376–381, https://doi.org/10.1002/chem.201504035.
[108] Y. Liang, W. Lu, Gamma-irradiation synthesis of -Fe3 O4/rGO nanocomposites as lithium-ion battery anodes, J. Mater. Sci. Mater. Electron. 31 (2020) 17075–17083, https://doi.org/10.1007/s10854-020-04268-9.
[109] R. Kumar, S.M. Youssry, E. Joanni, S. Sahoo, G. Kawamura, A. Matsuda, Microwave-assisted synthesis of iron oxide homogeneously dispersed on reduced graphene oxide for high-performance supercapacitor electrodes, J. Energy Storage. 56 (2022) 105896, https://doi.org/10.1016/j.est.2022.105896.
[110] C.M. Kavitha, K.M. Eshwarappa, M.P. Shilpa, S.J. Shetty, S. Surabhi, A. P. Shashidhar, N. Karunakara, S.C. Gurumurthy, G. Sanjeev, Tuning the optical and electrical properties by gamma irradiation of silver nanoparticles decorated graphene oxide on glutaraldehyde crosslinked polyvinyl alcohol matrix, Mater. Res. Bull. 173 (2024) 112685, https://doi.org/10.1016/j.materresbull.2024.112685.
[111] G.V. Kumar, R. Chandramani, Investigations on Fe 3+ doped polyvinyl alcohol films with and without gamma (γ)-irradiation, Appl. Surf. Sci. 255 (2009) 7047–7050, https://doi.org/10.1016/j.apsusc.2009.03.038.
[112] H.J. Salavagione, G. Martı, A. g,, Synthesis of poly (vinyl alcohol)/reduced graphite oxide nanocomposites with improved thermal and electrical properties, J. Mater. Chem. 19 (2009) 5027–5032, https://doi.org/10.1039/b904232f.
[113] X. Yang, L. Li, S. Shang, X. Tao, Synthesis and characterization of layer-aligned poly (vinyl alcohol)/graphene nanocomposites, Polymer (guildf). 51 (2010) 3431–3435, https://doi.org/10.1016/j.polymer.2010.05.034.
[114] A.T. Naikwadi, B.K. Sharma, K.D. Bhatt, Gamma Radiation Processed Polymeric Materials for High Performance Applications : A Review, Front. Chem. 10 (2022) 1–15, https://doi.org/10.3389/fchem.2022.837111.
[115] A. Massoud, O.M. Farid, R.M. Maree, K.F. Allan, Z.R. Tian, An improved metal cation capture on polymer with graphene oxide synthesized by gamma radiation, React. Funct. Polym. 151 (2020) 104564, https://doi.org/10.1016/j.reactfunctpolym.2020.104564.
[116] J.R. Ramya, K.T. Arul, P. Sathiamurthi, E.A.K. Nivethaa, S. Baskar, S. Amudha, B. Mohana, K. Elayaraja, S. Chandra, K. Asokan, S.N. Kalkura, Gamma irradiated poly (methyl methacrylate)-reduced graphene oxide composite thin films for multifunctional applications, Compos. Part B 163 (2019) 752–760, https://doi.org/10.1016/j.compositesb.2019.01.041.
[117] D. Ajay, G. Anshika, P. Sangeeta, K. Mukesh, Synthesis and Characterization of Gamma Irradiated Graphene Oxide-Polypyrrole Nanocomposites, J. Phys. Conf. Ser. (2020) 012034, https://doi.org/10.1088/1742-6596/1531/1/012034.
[118] Y. Shi, D. Xiong, J. Li, N. Wang, In Situ Reduction of Graphene Oxide Nanosheets in Poly(vinyl alcohol) Hydrogel by γ-Ray Irradiation and Its Influence on Mechanical and Tribological Properties, J. Phys. Chem. c. 120 (2016) 19442–19453, https://doi.org/10.1021/acs.jpcc.6b05948.
[119] D. Swantomo, K.T. Basuki, Y. Yunus, Preparation of Graphene-Polyaniline-Cellulose Double Network Hydrogels Using One Pot Method by Gamma Irradiation with Electrochemical Properties, Indones. J. Chem. 18 (2018) 411–420, https://doi.org/10.22146/ijc.30467.
[120] V. Gupta, N. Miura, Influence of the microstructure on the supercapacitive behavior of polyaniline/single-wall carbon nanotube composites, J. Power Sources. 157 (2006) 616–620, https://doi.org/10.1016/j.jpowsour.2005.07.046.
[121] S.A. Zikalala, R. Selvaraj, F. Al Marzouqi, A.T. Kuvarega, B.B. Mamba, S. D. Mhlanga, E.N. Nxumalo, Amorphous carbon nanotube residue modification of solgel-synthesized C-, N-doped TiO2 for photocatalytic applications, J. Nanoparticle Res. 22 (2020), https://doi.org/10.1007/s11051-020-05089-x.
[122] S.S. Fiyadh, M.A. AlSaadi, W.Z. Jaafar, M.K. AlOmar, S.S. Fayaed, N.S. Mohd, L. S. Hin, A. El-Shafie, Review on heavy metal adsorption processes by carbon nanotubes, J. Clean. Prod. 230 (2019) 783–793, https://doi.org/10.1016/j.jclepro.2019.05.154.
[123] Z. Zhu, An Overview of Carbon Nanotubes and Graphene for Biosensing Applications, Nano-Micro Lett. 9 (2017) 1–24, https://doi.org/10.1007/s40820-017-0128-6.
[124] M. Sun, G. Wang, X. Li, C. Li, Irradiation preparation of reduced graphene oxide/carbon nanotube composites for high-performance supercapacitors, J. Power Sources. 245 (2014) 436–444, https://doi.org/10.1016/j.jpowsour.2013.06.145.
[125] Y. Hwang, M. Kim, J. Kim, Enhancement of thermal and mechanical properties of flexible graphene oxide/carbon nanotube hybrid films though direct covalent bonding, J Mater Sci. 48 (2013) 7011–7021, https://doi.org/10.1007/s10853-013-7510-7.
[126] Q. Li, B. Guo, J. Yu, J. Ran, B. Zhang, H. Yan, J.R. Gong, Highly Efficient Visible-Light-Driven Photocatalytic Hydrogen Production of CdS-Cluster-Decorated Graphene Nanosheets, Am. Chem. Soc. 133 (2011) 10878–10884.
[127] L. Shahriary, H. Ghourchian, A.A. Athawale, Graphene-Multiwalled Carbon Nanotube Hybrids Synthesized by Gamma Radiations : Application as a Glucose Sensor, J. Nanotechnol. (2014) 1–10, https://doi.org/10.1155/2014/903872.
[128] V. Mani, B. Devadas, S.M. Chen, Direct electrochemistry of glucose oxidase at electrochemically reduced graphene oxide-multiwalled carbon nanotubes hybrid material modified electrode for glucose biosensor, Biosens. Bioelectron. 41 (2013) 309–315, https://doi.org/10.1016/j.bios.2012.08.045.
[129] H. Ma, L. Zhang, Y. Zhang, S. Wang, C. Sun, H. Yu, X. Zeng, M. Zhai, Radiation preparation of graphene/carbon nanotubes hybrid fillers for mechanical reinforcement of poly (vinyl alcohol) films, Radiat. Phys. Chem. 118 (2016) 21–26, https://doi.org/10.1016/j.radphyschem.2015.03.028.
[130] H. Zhou, S. Bai, Y. Zhang, D. Xu, M. Wang, Recent Advances in Ionic Liquids and Ionic Liquid-Functionalized Graphene: Catalytic Application and Environmental Remediation, Int. J. Environ. Res. Public Health. 19 (2022), https://doi.org/10.3390/ijerph19137584.
[131] J. Kim, S. Kim, Preparation and electrochemical property of ionic liquid-attached graphene nanosheets for an application of supercapacitor electrode, Electrochim. Acta. 119 (2014) 11–15, https://doi.org/10.1016/j.electacta.2013.11.187.
[132] J. Du, K. Xu, X. Yang, Z. Dong, L. Zhao, Removal of diclofenac sodium from aqueous solution using different ionic liquids functionalized tragacanth gum hydrogel prepared by radiation technique, Int. J. Biol. Macromol. 265 (2024) 130758, https://doi.org/10.1016/j.ijbiomac.2024.130758.
[133] T.Y. Kim, H.W. Lee, J.E. Kim, K.S. Suh, Synthesis of phase transferable graphene sheets using ionic liquid polymers, ACS Nano. 4 (2010) 1612–1618, https://doi.org/10.1021/nn901525e.
[134] G.F.L. Pereira, R.G. Pereira, M. Salanne, L.J.A. Siqueira, Molecular Dynamics Simulations of Ether-Modified Phosphonium Ionic Liquid Confined in between Planar and Porous Graphene Electrode Models, J. Phys. Chem. c. 123 (2019) 10816–10825, https://doi.org/10.1021/acs.jpcc.9b01821.
[135] W. Guo, S.M. Mahurin, R.R. Unocic, H. Luo, S. Dai, Broadening the gas separation utility of monolayer nanoporous graphene membranes by an ionic liquid gating, Nano Lett. 20 (2020) 7995–8000, https://doi.org/10.1021/acs.nanolett.0c02860.
[136] T.T. Tung, M. Castro, T.Y. Kim, K.S. Suh, J.F. Feller, High stability silver nanoparticles-graphene/poly(ionic liquid)-based chemoresistive sensors for volatile organic compounds' detection Chemosensors and Chemoreception, Anal. Bioanal. Chem. 406 (2014) 3995–4004, https://doi.org/10.1007/s00216-013-7557-y.
[137] M. Zhang, X. Ma, J. Li, R. Huang, L. Guo, X. Zhang, Y. Fan, X. Xie, G. Zeng, Enhanced removal of As(III) and As(V) from aqueous solution using ionic liquid-modified magnetic graphene oxide, Chemosphere. 234 (2019) 196–203, https://doi.org/10.1016/j.chemosphere.2019.06.057.
[138] O.P. Khatri, K. Adachi, K. Murase, K.I. Okazaki, T. Torimoto, N. Tanaka, S. Kuwabata, H. Sugimura, Self-assembly of ionic liquid (BMI-PF6)-stabilized gold nanoparticles on a silicon surface: Chemical and structural aspects, Langmuir. 24 (2008) 7785–7792, https://doi.org/10.1021/la800678m.
[139] S. Wang, Y. Zhang, H.L. Ma, Q. Zhang, W. Xu, J. Peng, J. Li, Z.Z. Yu, M. Zhai, Ionic-liquid-assisted facile synthesis of silver nanoparticle-reduced graphene oxide hybrids by gamma irradiation, Carbon n. y. 55 (2013) 245–252, https://doi.org/10.1016/j.carbon.2012.12.033.
[140] G. Yang, N. Song, F. Deng, J. Liang, Q. Huang, J. Dou, Y. Wen, M. Liu, X. Zhang, Y. Wei, Direct surface functionalization of graphene oxide with ionic liquid through gamma ray irradiation induced radical polymerization with remarkable enhanced adsorption capacity, J. Mol. Liq. 306 (2020) 112877, https://doi.org/10.1016/j.molliq.2020.112877.
[141] E. Samiei, S. Mohammadi, M. Torkzadeh-Mahani, Effect of gamma-irradiation on electrochemical properties of ZnCo2O4-rGO for supercapacitor application, Diam. Relat. Mater. 127 (2022) 109157, https://doi.org/10.1016/j.diamond.2022.109157.
[142] Q. Zhang, S. Ye, X. Song, S. Luo, Photocatalyst based on TiO 2 nanotube arrays co-decorated with CdS quantum dots and reduced graphene oxide irradiated by γ rays for effective degradation of ethylene, Appl. Surf. Sci. 442 (2018) 245–255, https://doi.org/10.1016/j.apsusc.2018.02.139.
[143] B. Li, Y. Feng, K. Ding, G. Qian, X. Zhang, J. Zhang, The effect of gamma ray irradiation on the structure of graphite and multi-walled carbon nanotubes, Carbon n. y. 60 (2013) 186–192, https://doi.org/10.1016/j.carbon.2013.04.012.
[144] D.H. Galván, I.L. Garzón, P. Santiago, Structural Changes and Electronic Properties of Gamma Irradiated Graphite : An Experimental and Theoretical Study, Fuller. Sci. Technol. 6 (1998) 867–883, https://doi.org/10.1080/10641229809350245.
[145] D.C. Clifford, C.E. Castano, J.V. Rojas, Supported transition metal nanomaterials: Nanocomposites synthesized by ionizing radiation, Radiat. Phys. Chem. 132 (2017) 52–64, https://doi.org/10.1016/j.radphyschem.2016.12.001.
[146] T. Kimio, K. Gejendran, Nanao, Relative biological effectiveness (RBE) and dose rate dependent ratio of translocation to dicentric chromosome yield in 252Cf neutrons, Indian J. Sci. Technol. 2 (2009) 1–11.
[147] D. Hao, Y. Yang, B. Xu, Z. Cai, Bifunctional Fabric with Photothermal E ff ect and Photocatalysis for Highly E ffi cient Clean Water Generation, (2018). 10.1021/acssuschemeng.8b02094.

[148] N.E. Zikalala, S. Azizi, S.A. Zikalala, I. Kamika, M. Maaza, A.A. Zinatizadeh, T. Mokrani, K. Kaviyarasu, An Evaluation of the Biocatalyst for the Synthesis and Application of Zinc Oxide Nanoparticles for Water Remediation—A Review, Catalysts. 12 (2022), https://doi.org/10.3390/catal12111442.
[149] M. Rafique, R. Tahir, S.S.A. Gillani, M.B. Tahir, M. Shakil, T. Iqbal, M. O. Abdellahi, Plant-mediated green synthesis of zinc oxide nanoparticles from Syzygium Cumini for seed germination and wastewater purification, Int. J. Environ. Anal. Chem. 00 (2020) 1–16, https://doi.org/10.1080/03067319.2020.1715379.
[150] S.A. Zikalala, M.B. Chabalala, N.N. Gumbi, N.J. Coville, B.B. Mamba, B. K. Mutuma, E.N. Nxumalo, Microwave-assisted synthesis of titania-amorphous carbon nanotubes/amorphous nitrogen-doped carbon nanotubes nanohybrids for photocatalytic degradation of textile wastewater, RSC Adv. 11 (2021) 6748–6763, https://doi.org/10.1039/d0ra08191d.
[151] S.A. Zikalala, R. Selvaraj, F. Al Marzouqi, A.T. Kuvarega, B.B. Mamba, S. D. Mhlanga, E.N. Nxumalo, Tailoring TiO2through N doping and incorporation of amorphous carbon nanotubes via a microwave-assisted hydrothermal method, J. Environ Chem. Eng. 8 (2020) 104082, https://doi.org/10.1016/j.jece.2020.104082.
[152] K. Hareesh, R.P. Joshi, S.S. Dahiwale, V.N. Bhoraskar, S.D. Dhole, Synthesis of Ag-reduced graphene oxide nanocomposite by gamma radiation assisted method and its photocatalytic activity, Vaccum. 124 (2016) 40–45, https://doi.org/10.1016/j.vacuum.2015.11.011.
[153] A.A. Al-Kahtani, M.F. Abou Taleb, Photocatalytic degradation of Maxilon C.I. basic dye using CS/CoFe2O4/GONCs as a heterogeneous photo-Fenton catalyst prepared by gamma irradiation, J. Hazard. Mater. 309 (2016) 10–19, https://doi.org/10.1016/j.jhazmat.2016.01.071.
[154] X. Fu, Y. Zhang, P. Cao, H. Ma, P. Liu, L. He, J. Peng, J. Li, M. Zhai, Radiation synthesis of CdS/reduced graphene oxide nanocomposites for visible-light-driven photocatalytic degradation of organic contaminant, Radiat. Phys. Chem. 123 (2016) 79–86, https://doi.org/10.1016/j.radphyschem.2016.02.016.
[155] Q. Ke, J. Wang, Graphene-based materials for supercapacitor electrodes – A review, J. Mater. 2 (2016) 37–54, https://doi.org/10.1016/j.jmat.2016.01.001.
[156] K. Kakaei, M.D. Esrafili, A. Ehsani, Graphene-Based Electrochemical Supercapacitors, 2019. 10.1016/B978-0-12-814523-4.00009-5.
[157] S. Kalia, R. Kumar, R. Dhiman, R.K. Singh, Ion irradiation/implantation induced defect engineering and modification in graphene derivatives-based nanocomposites: Energy storage/conversion and sensor, J. Energy Storage. 83 (2024) 110650, https://doi.org/10.1016/j.est.2024.110650.
[158] J. Yan, Y. Xiao, G. Ning, T. Wei, Z. Fan, Facile and rapid synthesis of highly crumpled graphene sheets as high-performance electrodes for supercapacitors, RSC Adv. 3 (2013) 2566–2571, https://doi.org/10.1039/c2ra22685e.
[159] R. Kumar, S. Sahoo, E. Joanni, R.K. Singh, R.M. Yadav, R.K. Verma, D.P. Singh, W. K. Tan, A. Pérez del Pino, S.A. Moshkalev, A. Matsuda, A review on synthesis of graphene, h-BN and MoS2 for energy storage applications: Recent progress and perspectives, Nano Res. 12 (2019) 2655–2694, https://doi.org/10.1007/s12274-019-2467-8.
[160] B. Ankamwar, P. Das, U.K. Sur, Graphene–gold nanoparticle-based nanocomposites as an electrode material in supercapacitors, Indian J. Phys. 90 (2016) 391–397, https://doi.org/10.1007/s12648-015-0765-x.
[161] Q. Zhang, Y. Zhang, Z. Gao, S. Wang, J. Peng, J. Li, M. Zhai, A facile synthesis of platinum nanoparticle decorated graphene by one-step γ-ray induced reduction for high rate supercapacitors, J. Mater. Chem. c. 1 (2013) 321–328, https://doi.org/10.1039/c2tc00078d.
[162] M.M. Atta, M. Rabia, A.M. Elbasiony, E.O. Taha, M.M. Abdel Hamid, A.M. A. Henaish, Q. Zhang, Facile gamma-ray induced synthesis of reduced graphene oxide decorated with silver nanoparticles: a green approach for symmetric supercapacitor applications, Fullerenes Nanotub. Carbon Nanostructures. (2023) 1–10, https://doi.org/10.1080/1536383X.2023.2292705.
[163] M. Lu, Y. Yan, Y. Zheng, W. Zhang, X. He, Z. Wu, T. Yang, X. Xia, H. Huang, Y. Xia, Y. Gan, J. Zhang, Recent advances of aqueous rechargeable lithium/sodium ion batteries: key electrode materials and electrolyte design strategies, Mater. Today Energy. 38 (2023) 101454, https://doi.org/10.1016/j.mtener.2023.101454.
[164] S.K. Tiwari, S. Sahoo, N. Wang, A. Huczko, Graphene research and their outputs: Status and prospect, J. Sci. Adv. Mater. Devices. 5 (2020) 10–29, https://doi.org/10.1016/j.jsamd.2020.01.006.
[165] K. Il, J. Hyeri, K. Hee, S. Jeong, J. Kee, S. Hwan, O. Seok, H. Song, H. Kim, Gamma-ray irradiated graphene nanosheets/polydopamine hybrids as a superior anode material for lithium-ion batteries, Carbon Lett. 32 (2022) 305–312, https://doi.org/10.1007/s42823-021-00308-4.
[166] J. Jang, S.H. Song, H. Kim, J. Moon, H. Ahn, K. Il Jo, J. Bang, H. Kim, J. Koo, Janus Graphene Oxide Sheets with Fe3O4Nanoparticles and Polydopamine as Anodes for Lithium-Ion Batteries, ACS Appl, Mater. Interfaces. 13 (2021) 14786–14795, https://doi.org/10.1021/acsami.1c02892.
[167] S. Kalia, R. Kumar, R. Sharma, S. Kumar, D. Singh, R.K. Singh, Two-dimensional layered rGO-MoS2 heterostructures decorated with Fe3O4 nanoparticles as an electrochemical sensor for detection of para-nitrophenol, J. Phys. Chem. Solids. 184 (2024) 111719, https://doi.org/10.1016/j.jpcs.2023.111719.
[168] Z. Wang, F. Li, J. Xia, L. Xia, F. Zhang, S. Bi, G. Shi, Y. Xia, J. Liu, Y. Li, L. Xia, An ionic liquid-modified graphene based molecular imprinting electrochemical sensor for sensitive detection of bovine hemoglobin, Biosens. Bioelectron. 61 (2014) 391–396, https://doi.org/10.1016/j.bios.2014.05.043.
[169] H. Hashtroudi, R. Kumar, R. Savu, S. Moshkalev, G. Kawamura, A. Matsuda, M. Shafiei, Hydrogen gas sensing properties of microwave-assisted 2D Hybrid Pd/rGO: Effect of temperature, humidity and UV illumination, Int. J. Hydrogen Energy. 46 (2021) 7653–7665, https://doi.org/10.1016/j.ijhydene.2020.11.268.
[170] X. Li, L. Liu, Z. Xu, W. Wang, J. Shi, L. Liu, M. Jing, F. Li, Chemical Gamma irradiation and microemulsion assisted synthesis of monodisperse flower-like platinum-gold nanoparticles / reduced graphene oxide nanocomposites for ultrasensitive detection of carcinoembryonic antigen, Sensors Actuators b. Chem. 287 (2019) 267–277, https://doi.org/10.1016/j.snb.2019.02.026.
[171] N. Passornraprasit, T. Siripongpreda, S. Ninlapruk, Irradiation crosslinking of graphene oxide/cellulose nanofiber/poly (acrylic acid) hydrogel as a urea sensing patch, Int. J. Biol. Macromol. 213 (2022) 1037–1046, https://doi.org/10.1016/j.ijbiomac.2022.06.053.
[172] S. Jovanovi, D. Jovanovi, G. Ciasca, M. Budimir, A. Bonasera, M. Scopelliti, O. Markovi, B. Todorovi, Gamma irradiation of graphene quantum dots with ethylenediamine : Antioxidant for ion sensing, Ceram. Int. 46 (2020) 23611–23622, https://doi.org/10.1016/j.ceramint.2020.06.133.
[173] Z. Wang, Z.F. Fan, Cu2 + modulated nitrogen-doped grapheme quantum dots as a turn-off/on fluorescence sensor for the selective detection of histidine in biological fluid, Spectrochim. Acta - Part A Mol. Biomol. Spectrosc. 189 (2018) 195–201, https://doi.org/10.1016/j.saa.2017.08.003.
[174] X. Zou, L. Zhang, Z. Wang, Y. Luo, Mechanisms of the Antimicrobial Activities of Graphene Materials, J. Am. Chem. Soc. 138 (2016) 2064–2077, https://doi.org/10.1021/jacs.5b11411.
[175] X. Cai, S. Tan, M. Lin, A. Xie, W. Mai, X. Zhang, Z. Lin, T. Wu, Y. Liu, Synergistic antibacterial brilliant blue/reduced graphene oxide/quaternary phosphonium salt composite with excellent water solubility and specific targeting capability, Langmuir. 27 (2011) 7828–7835, https://doi.org/10.1021/la201499s.
[176] N.E. Zikalala, S.A. Zikalala, S. Azizi, I.A. Kamika, E.N. Nxumalo, A.A. Zinatizadeh, E.M.N. Chirwa, M. Maaza, The Role of Inorganic and Carbon Nanomaterials in Surface Modification to Attain Antibiofouling Polymeric Membranes for Water Treatment—A Review, Ind. Eng. Chem. Res. 62 (2023) 9354–9380, https://doi.org/10.1021/acs.iecr.3c00400.
[177] S. Liu, T.H. Zeng, M. Hofmann, E. Burcombe, J. Wei, R. Jiang, J. Kong, Y. Chen, Antibacterial activity of graphite, graphite oxide, graphene oxide, and reduced graphene oxide: Membrane and oxidative stress, ACS Nano. 5 (2011) 6971–6980, https://doi.org/10.1021/nn202451x.
[178] A. Nayamadi Mahmoodabadi, A. Kompany, M. Mashreghi, Characterization, antibacterial and cytotoxicity studies of graphene-Fe3O4 nanocomposites and Fe3O4 nanoparticles synthesized by a facile solvothermal method, Mater. Chem. Phys. 213 (2018) 285–294, https://doi.org/10.1016/j.matchemphys.2018.04.033.
[179] R.A. Mostafa, I.M. El-sherbiny, N.S. Selim, A.M. Sallam, H.A. Ashry, Green synthesis of strontium-reduced graphene oxide biocomposite using gamma radiation, Radiat. Phys. Chem. 197 (2022) 110109, https://doi.org/10.1016/j.radphyschem.2022.110109.
[180] R.M. Fathy, A.Y. Mahfouz, Eco-friendly graphene oxide-based magnesium oxide nanocomposite synthesis using fungal fermented by-products and gamma rays for outstanding antimicrobial, antioxidant, and anticancer activities, J. Nanostructure Chem. 11 (2021) 301–321, https://doi.org/10.1007/s40097-020-00369-3.
[181] D. Zhang, S. Yang, Y. Chen, S. Liu, H. Zhao, J., Gu, γ -ray Irradiation Crosslinking of Chitosan / Graphene Oxide Composite Film : Swelling, Thermal Stability, Mechanical, and Polymers (basel) 10 (2018) 1–14, https://doi.org/10.3390/polym10030294.
[182] S. Sivaselvam, R. Selvakumar, C. Viswanathan, N. Ponpandian, Rapid one-pot synthesis of PAM-GO-Ag nanocomposite hydrogel by gamma-ray irradiation for remediation of environment pollutants and pathogen inactivation, Chemosphere. 275 (2021) 130061, https://doi.org/10.1016/j.chemosphere.2021.130061.
[183] M. Budimir, Z. Marković, J. Vajdak, S. Jovanović, P. Kubat, P. Humpoliček, M. Mičušik, M. Danko, A. Barras, D. Milivojević, Z. Špitalsky, R. Boukherroub, B. T. Marković, Enhanced visible light-triggered antibacterial activity of carbon quantum dots/polyurethane nanocomposites by gamma rays induced pre-treatment, Radiat. Phys. Chem. 185 (2021), https://doi.org/10.1016/j.radphyschem.2021.109499.
[184] S. Duan, Y. Hu, Y. Zhao, K. Tang, Z. Zhang, Z. Liu, Y. Wang, H. Guo, Y. Miao, H. Du, D. Yang, S. Li, J. Zhang, Nanomaterials for photothermal cancer therapy, RSC Adv. 13 (2023) 14443–14460, https://doi.org/10.1039/d3ra02620e.
[185] N. Tsolekile, V. Ncapayi, S. Parani, E.H.M. Sakho, M.C. Matoetoe, S.P. Songca, O. S. Oluwafemi, Synthesis of fluorescent CuInS2/ZnS quantum dots - Porphyrin conjugates for photodynamic therapy, MRS Commun. 8 (2018) 398–403, https://doi.org/10.1557/mrc.2018.60.
[186] X. Dong, Z. Zhu, Q. Sun, H. Zhang, C. Yang, Chitosan functionalized gold nanostars as a theranostic platform for intracellular microRNA detection and photothermal therapy, J. Mater. Chem. b. 11 (2023) 11082–11093, https://doi.org/10.1039/d3tb02029k.
[187] T.C. Lebepe, S. Parani, V. Ncapayi, R. Maluleke, G.I.M. Mbaz, O.T. Fanoro, J. R. Varghese, A. Komiya, T. Kodama, O.S. Oluwafemi, Graphene oxide-gold nanorods nanocomposite-porphyrin conjugate as promising tool for cancer phototherapy performance, Pharmaceuticals. 14 (2021), https://doi.org/10.3390/ph14121295.
[188] S. Ahirwar, S. Mallick, D. Bahadur, Photodynamic therapy using graphene quantum dot derivatives, J. Solid State Chem. 282 (2020) 121107, https://doi.org/10.1016/j.jssc.2019.121107.
[189] D.P. Kepi, A.M. Stefanovi, M.D. Budimir, V.B. Pavlovi, B. Aurelio, S. Michalengelo, B.M.T. Markovic, Gamma rays induced synthesis of graphene oxide / gold nanoparticle composites : structural and photothermal study, Radiat.

Phys. Chem. J. 202 (2023) 110545, https://doi.org/10.1016/j.radphyschem.2022.110545.

[190] K. DP, K.D. N, M.Z. M, V.B. Pavlovi, D.J. Jovanovi, B.M. Todorovi, One-step preparation of gold nanoparticles - exfoliated graphene composite by gamma irradiation at low doses for photothermal therapy applications, Mater. Charact. 173 (2021) 110944. 10.1016/j.matchar.2021.110944.

[191] S.P. Jovanović, Z. Syrgiannis, Z.M. Marković, A. Bonasera, D.P. Kepić, M. D. Budimir, D.D. Milivojević, V.D. Spasojević, M.D. Dramićanin, V.B. Pavlović, B. m., Todorović Marković, Modification of Structural and Luminescence Properties of Graphene Quantum Dots by Gamma Irradiation and Their Application in a Photodynamic Therapy, ACS Appl, Mater. Interfaces. 7 (2015) 25865–25874, https://doi.org/10.1021/acsami.5b08226.

[192] B. Gupta, A.A. Melvin, T. Matthews, S. Dash, A.K. Tyagi, Facile gamma radiolytic synthesis of synergistic Co3O4-rGO nanocomposite: direct use in photocatalytic water splitting, Mater. Res. Express. 1 (2014) 045507, https://doi.org/10.1088/2053-1591/1/4/045507.

[193] N. Ubaidah, T. Choo, R. Mohamad, N. Mat, K. Ying, W. Yin, K. Long, One-pot gamma radiolysis synthesis of a graphene oxide-supported cobalt oxyhydroxide electrocatalyst for oxygen reduction reaction, Radiat. Phys. Chem. 205 (2023) 110680, https://doi.org/10.1016/j.radphyschem.2022.110680.